To the Graduate Council:

I am submitting herewith a thesis written by Joshua David Scholes entitled "Bio-derived Fuels for Hybrid Rocket Motors." I have examined the final paper copy of this thesis for form and content and recommend that it be accepted in partial fulfillment of the requirements for the degree of Master of Science, with a major in Aerospace Engineering.

Evans Lyne, Major Professor

We have read this thesis
and recommend its acceptance:

Accepted for the Council:

Vice Chancellor and
Dean of Graduate Students

Bio-derived Fuels for Hybrid Rocket Motors

A Thesis Presented for the Master of Science Degree
The University of Tennessee, Knoxville

Joshua David Scholes
December 2005

Acknowledgements
I would first like to thank God for life, salvation, and making this opportunity possible.

I would like to thank Dr. Evans Lyne for support of this research and for his guidance regarding various aspects of it as well as his encouragement.
I would also like to thank Dr. Mancil Milligan and Dr. Robert Bond for serving on the committee and for their teaching throughout the years. I would also like to thank Dr. Viatcheslav Naoumov for his help with the theoretical work and data analysis.
A special thanks goes to my testing partner, Capt. Scott Putnam, for all of his help and making the research more enjoyable.
I would also like to thank my peers from my senior group and the senior group that worked under me: David Austin, Ben Elton, Cliff Combs, Meghan Dodge, Paul Wozniak, Stephen Dzialo, Jeff Jostworth, Mary Pardue, Jiten Patel, Henry Simington, and Steven Wright.

Other thanks:
Dr. Butch Irick for use in storage of the facility
Dennis Higdon for his expert help in instrumentation
David Gray and the AirGas Company for their help in countless hardware purchases
My family, Terry, Linda, and Emily Scholes, for always supporting me
Calvary Baptist Church

ABSTRACT

Two bio-derived fuels have been successfully tested in a laboratory scale hybrid rocket combustion chamber located at the University of Tennessee, Knoxville. Pure lard soaked in an open cell sponge matrix and beeswax were both tested, using gaseous oxygen as the oxidizer. Given similar testing conditions, these fuels exhibit higher regression rates than the common hybrid rocket propellant HTPB (hydroxyl-terminated polybutadiene), thus overcoming one of the main shortcomings of hybrid rocket fuels. These fuels also have similar or higher regression rates than paraffin-based fuels recently tested by a Stanford University/NASA Ames team. Measured thrusts ranged from 20-140 Newtons, and calculated specific impulses ranged from 60-160 seconds. All tests were excessively fuel-rich, and this leads to decreased combustion temperature and specific impulse. It is likely that this is caused by a shorter than optimal mixing chamber. This study concludes that these fuels are worth further study and could prove useful to practical application in rocketry.

Table of Contents

List of Tables

List of Figures

Nomenclature

a	Power curve coefficient
A_e	Exit area (m^2)
A_t	Orifice plate hole area (m^2)
C	Discharge coefficient
d	Orifice plate hole diameter (m)
D	Pipe diameter (m)
d_b	Bolt diameter (m)
D_f	Final port diameter (m)
e	Gas expansion coefficient
g	Acceleration due to gravity at the earth's surface (m/sec^2)
G_{ox}	Average oxidizer mass flux (g/cm^2-sec)
I	Total impulse (N-sec)
ID	Inner diameter (m)
I_{sp}	Specific impulse (sec)
K	Gas isentropic exponent
L_g	Grain length (m)
m	Mass (kg)
$\dot{m}_f$	Average fuel mass flow rate (kg/sec)
M_f	Burned fuel mass (kg)
M_{final}	Final Mass (kg)
$M_{initial}$	Initial mass (kg)
$\dot{m}_{ox}$	Average oxidizer mass flow rate (kg/sec)
$\dot{m}_p$	Average propellant mass flow rate (kg/sec)
M_p	Burned propellant mass (kg)
n	Power curve exponent
No_b	Number of bolts
OD	Grain outer diameter (m)
O/F	Oxidizer to fuel ratio
$(O/F)_{stoich}$	Stoichiometric O/F value
P_a	Ambient pressure (psia)
P_c	Average combustion pressure (psig)
P_e	Exit Pressure (psig)
P_{up}	Average upstream orifice plate pressure (psig)
$\dot{r}$	Average regression rate (m/sec)
Re_D	Reynolds Number
R_u	Universal gas constant (J/kmol-K)

t	Time (sec)
T	Average thrust (N)
T_c	Combustion temperature (K)
T_{ox}	Oxidizer Temperature (K)
t_b	Burn time (sec)
t_{g_i}	Initial grain thickness (m)
t_{g_f}	Final grain thickness (m)
t_s	Case thickness (m)
u_e	Exit velocity (m/sec)
u_{eq}	Equivalent exit velocity (m/sec)
V	Volume (m^3)
β	Beta ratio
ΔP	Average pressure differential
ϕ	Equivalence ratio
γ	Specific heat ratio
μ_{ox}	Molecular mass of oxidizer (kg/kmol)
μ_f	Molecular mass of fuel (kg/kmol)
ρ	Density (kg/m^3)
σ_a	Axial stress (psi)
σ_b	Bolt stress (psi)
σ_h	Hoop stress (psi)

I. INTRODUCTION

Hybrid rockets generally employ a solid fuel and a liquid or gaseous oxidizer. Reverse hybrids are less common and are just the opposite, with a solid oxidizer and a liquid fuel. Looking at the solid fuel type, an oxidizer is injected at high pressure into a combustion chamber that houses the fuel grain. The flow of vaporized oxidizer over the solid fuel surface creates a boundary layer. The flame zone lies inside this boundary layer. The oxidizer diffuses into the flame zone and the fuel enters through vaporization at the solid fuel wall surface (1).

Hybrids have some distinct advantages over traditional solid and liquid propelled rockets. First, hybrid rockets are safer than many traditional rockets because of the nearly nonexistent possibility of explosion. Hybrid fuels can be handled more easily because they are inert. Hybrid motors also have start-stop-restart capabilities unlike solids, which must continue burning until completion. They are also more flexible because of the throttleability. This is accomplished by regulating the flow of the oxidizer. These systems are also low cost. Furthermore, many fuel/oxidizer combinations have higher specific impulses than solid rocket motors and higher density-specific impulses than liquid propellant motors (1,2).

With these advantages also come some disadvantages. Hybrid fuels are known to have low regression rates. The mixture ratio, or oxidizer to fuel ratio, varies during combustion, so the specific impulse will also vary during combustion (2). Hybrids also have lower density-specific impulse than solid rocket motors. Unlike liquid motors, hybrids must retain some fuel in the combustion chamber at the end of the burn. This increases the motor mass fraction. Lastly, hybrids are still unproven in large-scale applications. Although they are thought to be useful for target missiles and applications with variable thrust requirements, hybrids are not comparable with large-scale solid or liquid propulsion systems.

Looking specifically at hybrids, one of the main characteristics of the fuel is its regression rate, or burn rate. In conventional fuels used in hybrids, e.g. HTPB and Plexiglas®, regression rates are less than one-third that of the propellants in solid motors.

With these low regression rates, more surface area must be created to allow for similar thrusts, so multiple port configurations are used. Here lies a problem with hybrid rockets. Fuels with low regression rates lead to increased fuel areas and more space requirements than fuels with high regression rates. There is also some structural compromise with these multi-port configurations because the grain is more liable to break off in chunks as the fuel burns. With higher regression rates, multi-port configurations would not be necessary as single or dual ports could be employed. The space requirement for a given mission would decrease with increasing regression rate as well. A joint study by Stanford University and NASA Ames discovered a class of paraffin-based fuels that yielded regression rates of around 3 times that of conventional hybrid fuels. It is theorized that the use of paraffin creates an unstable liquid layer and that droplets are located on the created liquid-gas interface (3,4). This increases surface area, and thus, regression rate. A desire to develop other fuels that have a high regression rate while employing non-toxic, bio-derived materials was a driving factor in this research.

There have been other recent studies on fuels for hybrid rockets. Many university studies have tested and launched vehicles using HTPB with either gaseous oxygen or nitrous oxide. Some of these teams are BYU, the University of Utah, Utah State University, the University of Illinois, and the University of Arkansas at Little Rock. The first private spacecraft, SpaceShipOne, is powered by a hybrid motor using HTPB and nitrous oxide (5).

There has been recent cause for concern because solid rocket propellant has found its way into ground water supplies in locations throughout the United States (6,7). With ground water affected, this in turn affects crops, animals, and drinking water. Traces of ammonium perchlorate have been found in lettuce and milk at various locales in the United States. It should be noted that perchlorate is naturally occurring, although most of it comes from a combination of testing and development of rockets, fireworks, and other explosives. A report by the Environmental Working Group, EWG, states that 90% of the perchlorate manufactured each year goes to the Air Force, NASA, and defense contractors to make rocket fuel (8). It also composes around 70% of space shuttle rocket motors. Perchlorate has been linked to thyroid problems, and the danger is more serious in children (9). The outcry from civilians in parts of California was loud enough to bring about some needed cleaning of the areas of the perchlorate excesses. For example, it is expected to cost $55 million to clean an Aerojet Superfund site in Rancho Cordova, California (8).

Given these circumstances, less toxic or non-toxic fuels are in demand. It is also desirable that these fuels be non-hazardous, so that they can be transported without special safety precautions. Thus, the aim of this research was to discover potential fuels that have high regression rates, are non-toxic, and non-hazardous. This research looked to two natural, bio-derived potential fuels, namely, lard and beeswax.

Lard was initially considered because it is known to have a high energy density, is readily available and inexpensive. Being three fatty acids linked to a molecule of glycerol, or triglyceride, makes for an energy density comparable to that of jet fuel (~43 MJ/kg). In initial thermodynamic analysis of lard combustion with gaseous oxygen, it was found that lard demonstrated the potential for high combustion temperatures and appropriate values of specific impulse. For example, combustion at a pressure of 30 atm operating at stoichiometric conditions provides a theoretical temperature of 3475 K and a vacuum specific impulse of 240 sec. These values are comparable to those for typical solid and hybrid propellants.

There were several specific objectives for this research. A primary goal was to determine the regression rate characteristics for lard in a sponge matrix and for beeswax. Regression rates were desired in relation to other parameters, namely, oxidizer flux rate and combustion pressure. These results are needed to allow future prediction of thrust levels and engine performance in order to design flight vehicles. A comparison of these fuels' regression characteristics to previous work was also desired. It was also a goal to analyze specific impulse and its relationship to equivalence ratio.

Chapter II will explain the test facility used. A brief history of the facility and improvements made will be presented as well as an overview of how the stand functions. Chapter III will discuss the results of the experimental testing of the fuels. Lastly, Chapter IV will give some general conclusions and recommendations for future work.

II. TEST FACILITY

History and Overview

The test facility used for this research was built in 2000 at the University of Tennessee, Knoxville to study Plexiglas®, a common hybrid rocket fuel. A senior design group in 2004 modified this test bench so that it could accommodate various fuels with the goal of successfully testing lard as a fuel. Another goal of this group was to upgrade the instrumentation and data collection systems. To verify these modifications, paraffin, a previously evaluated fuel, was tested. After verification, work proceeded with fuel testing, with continued facility upgrades. In 2005, work continued with additional facility improvements and continued testing of fuels with a shift in main testing from lard-based fuels to beeswax. A major goal of work in 2005 was to make the transition from a low-pressure test facility to a higher pressure test facility. This goal was accomplished with combustion pressures increasing from an average of 30 to 150 psig.

The fuel is housed in a case made from a 0.25-inch thick, 3-inch outer diameter, 10-inch long, steel pipe. This steel case is locked in place using a series of six turnbuckles, which act to preload the case between two steel caps. A sectional schematic of the combustion chamber assembly can be seen in Figure 1. The nozzle end cap houses a graphite converging-diverging conical nozzle. This nozzle has an exit area to throat area ratio of 2.75 and is designed for ideal expansion at a combustion pressure of 150 psig. The exit area is 0.22166 in^2. A converging nozzle with exit area of 0.15205 in^2 was used for nearly half the tests, as that was the nozzle in place from the existing test bench. The converging diverging nozzle was manufactured and installed in 2005 and has been in place since. The injector end steel cap houses injectors for the oxygen and propane supply as well as a spark plug. A detailed picture of the combustion chamber can be viewed in Figure 2. A restrictor plate is also located in this steel piece and is used to reduce the flowing oxidizer area to an area just greater than the initial port. An initial port diameter of 0.5-inch was used in every test. Oxygen is fed through this port and combustion is ignited using a shot of propane and a spark plug just upstream of the combustion chamber. A flow schematic is shown in Figure 3.

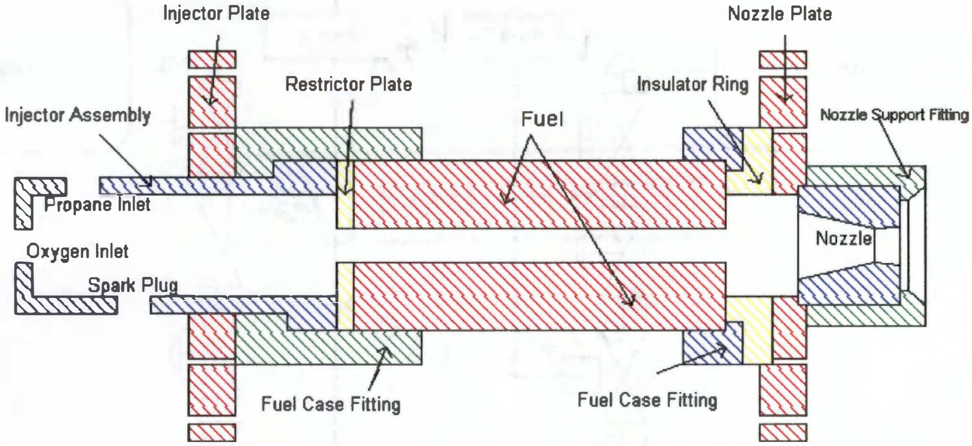

Figure 1: Sectional View of Combustion Chamber Assembly

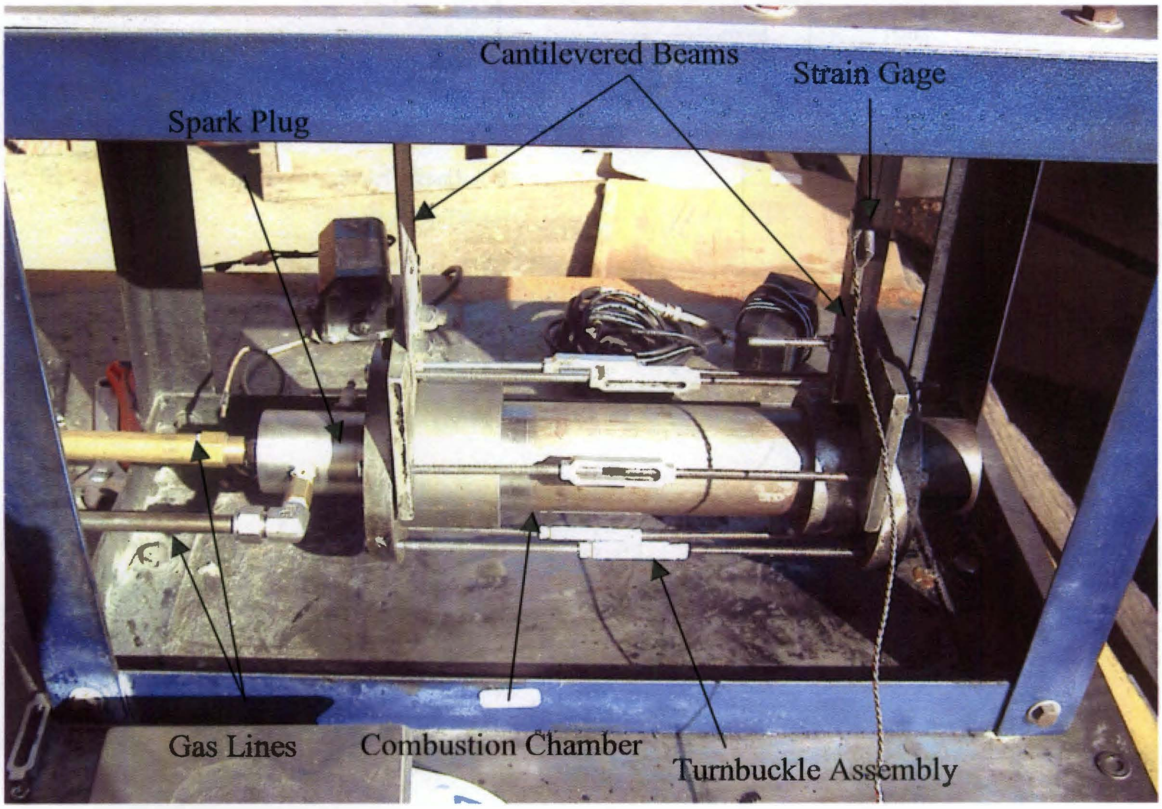

Figure 2: General Setup of Test Facility

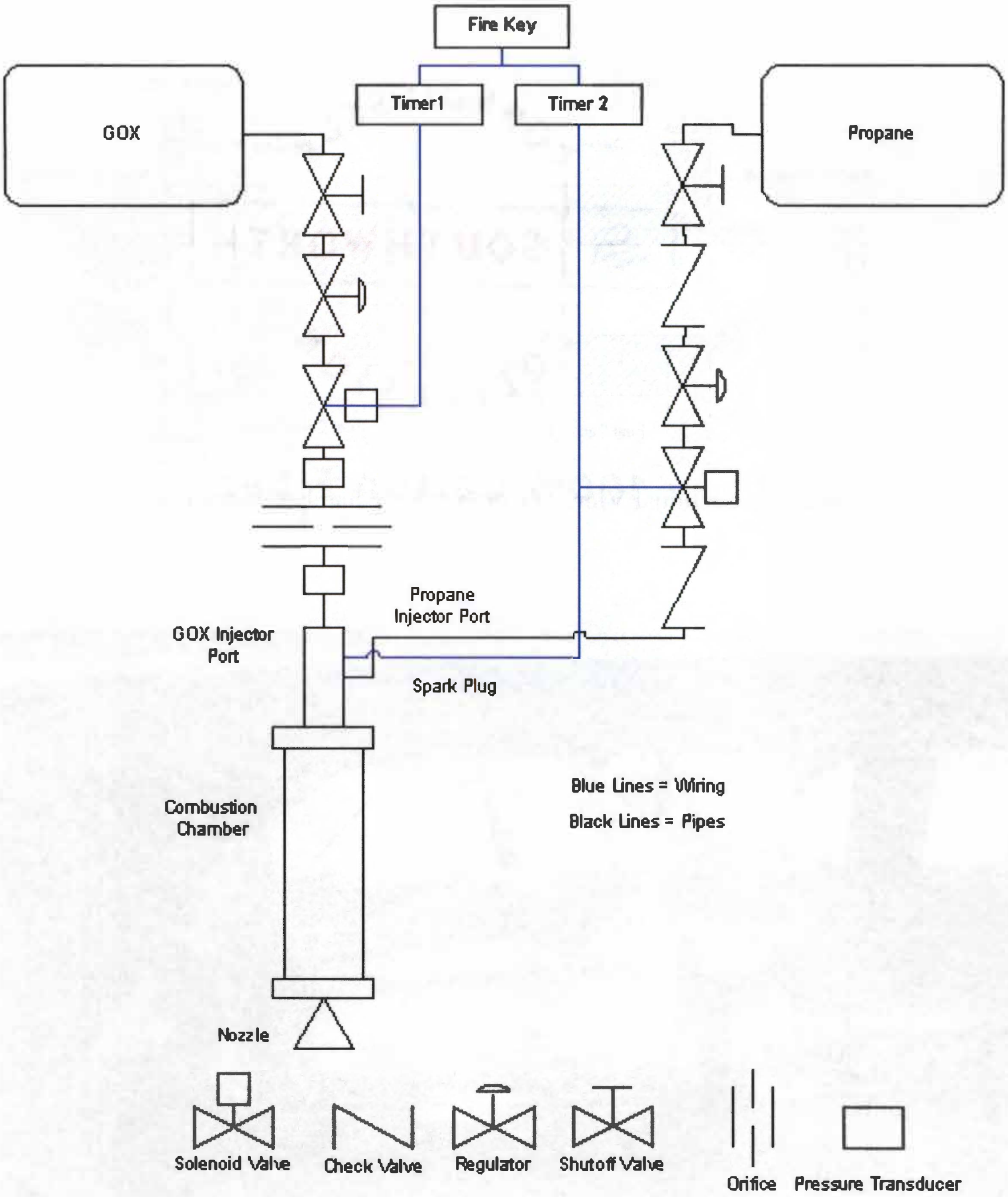

Figure 3: Flow Schematic of Test Facility

Timers control the duration of the test, with typical tests lasting from 5-7 seconds. Pressure regulators are used to set the oxygen and propane supply. These regulators are applied directly to the tanks. The oxygen has been regulated over a range of 50-450 psig, while the propane is always supplied at maximum, which tends to be around 80 psig. The supply pressure is not the same as the combustion pressure because of pressure losses in the pipes, across the orifice in the solenoid valve, and across the orifice plate for flow measurement. Around 350 psig must be supplied in order to achieve combustion pressures of around 150 psig. High-pressure tubing links the regulators to the solenoid valves. These solenoid valves are connected to the timers, and are used to control the flow of the gases. The gas lines are charged to desired pressures before the test by setting these desired values on the regulators. After the solenoid valves, the gases each flow through a 2 ft long, 0.5" diameter steel pipe, with the oxygen going through an orifice plate and then to the injectors and the propane going directly to the injectors.

Instrumentation

Data collected during the tests includes thrust, upstream orifice pressure, downstream orifice pressure, and change in fuel mass. Prior to 2005, the oxygen mass flow rate was determined using a pressure difference curve from the original test bench. This pressure drop was found using the difference between the set pressure on the oxygen regulator and the average combustion pressure. This method was deemed unsuitable for data analysis because of the uncertainty. It was a main goal of 2004 to employ a better method of determining the oxygen mass flow rate, and in late 2004, an orifice plate was installed to measure the flow rate more accurately. This orifice plate has pressure transducers located just upstream and downstream. The average pressure differential along with the average upstream pressure is used to find the average oxygen mass flow rate (10). A computer code was written in MATLAB and used to calculate a flow rate versus differential pressure chart. This code with detailed comments, the equations used, and a sample chart can be found in Appendix A. The downstream pressure is assumed to be the same value as the combustion pressure. This is assumed to be correct because this pressure and the pressure taken at the nozzle end of the combustion chamber were the same for all tests when a pressure transducer was previously installed at the end. No pressure transducer is currently being employed in the nozzle end cap because after the conversion to higher combustion pressures, these transducers failed every 1-2 tests. This failure was believed to be due to damage to the diaphragm in the transducer by high-pressure flame. Enough successful tests were performed with a pressure transducer located at the nozzle end to compare pressures and verify the assumption that combustion pressure is equivalent to the downstream orifice plate pressure. The thrust is also measured during each test. As viewed in Figure 1, the combustion chamber is supported on two cantilevered beams. The beam on the nozzle end has a strain gage. The strain gage was calibrated before each test using a standard series of weights added to a bucket. These weights covered the range of thrust during the tests. Since axial thrust is the exerted force, a pulley was used to simulate axial force on the system. A typical calibration plot with a linear approximation can be seen in Figure 4. A list of the weights used can be found after the calibration plot.

Each of the wired instrumentation devices is connected to a screw-pin box. This box is connected by cable to an analog to digital (A/D) converter card located in a computer. This card is 16 bit and has capabilities for 8 differential channels. Three channels were used, with two pressure transducers and one strain gage. Hewlett-Packard Visual Engineering Environment, or HP VEE, is used to collect the data. A screenshot of this program can be viewed in Appendix B with details following. The A/D card takes readings as counts, and these are converted to the desired value. This is done for both pressure transducers, and the output count value is converted to psig value. The strain gage count output is converted to volts, and the conversion to Newtons is done in Excel with the linear approximation from the calibration. The voltage range for the transducers is 1-5 Vdc, and the strain gage voltage range is 0-5 Vdc. The HP VEE program writes an Excel file with the data sorted into columns, including time. The data sampling rate is not constant, and it varies from around 16 Hz to 20 Hz.

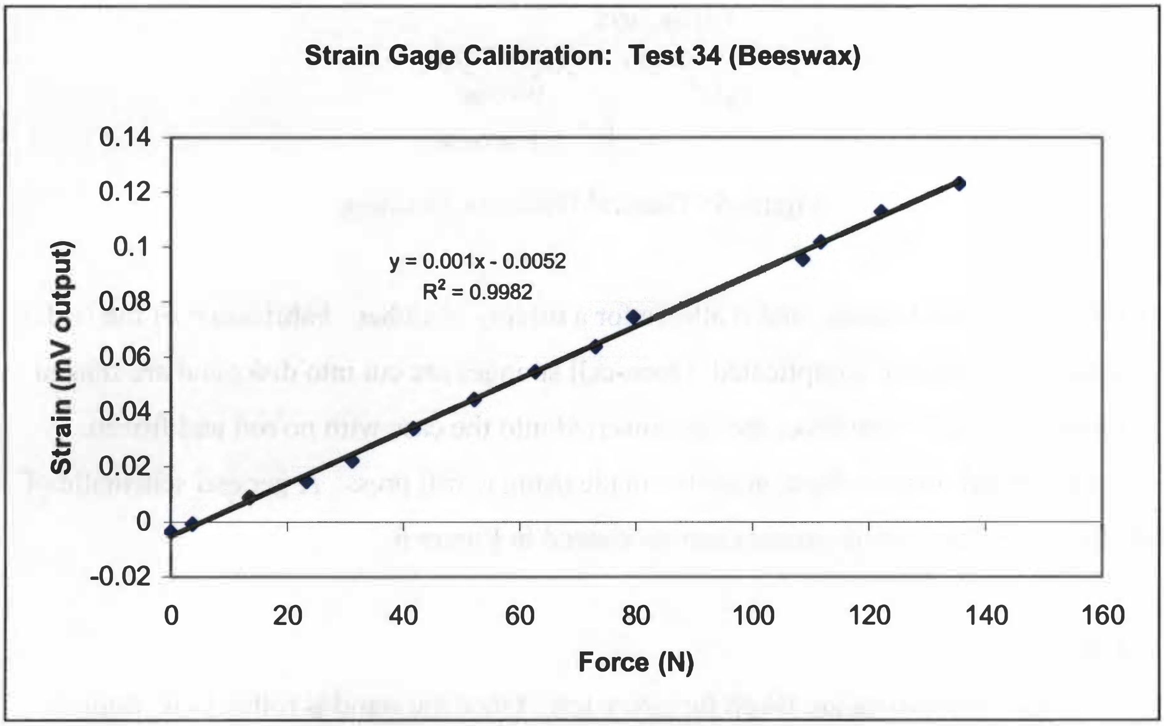

Figure 4: Strain Gage Calibration (Test 34)

Grain Fabrication

The melting temperatures for beeswax and lard are 63°C and 25°C, respectively. Chemical formulas are given as:

$$\text{Beeswax: } C_{46}H_{92}O_{10}$$

$$\text{Lard: } C_{15}H_{26}O_{6}$$

The molecular weights are 804 and 302, respectively. The densities are taken as 0.961 cc and 840 cc. Beeswax is a compound of several chemical compounds, predominantly compounds based on straight-chain monohydric alcohols with even numbered carbon chains (11). It has a general structure is shown in Figure 5 (12):

The fuel is liquefied in a pot on a hotplate, then poured into the case, and allowed to harden. The lard-based grains are then frozen because at room temperature lard is not hard enough to maintain the desired shape in the case. Beeswax is cooled to room temperature, as it is able to maintain the desired shape without being frozen. Half inch, polished, steel rods simulate the port and are placed in the middle of the case and removed after the fuel has hardened. The case and rod are inserted into a wooden cap with a depth of 0.5” prior to pouring. This depth is not filled as this end is considered

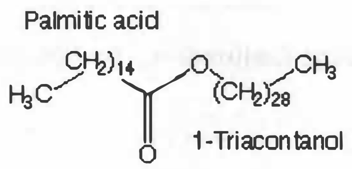

Figure 5: General Beeswax Structure

the aft end of the chamber, and it allows for a mixing chamber. Fabrication of the lard-sponge grains is more complicated. Open-cell sponges are cut into disks and are soaked in liquefied lard. These disks are then inserted into the case with no rod and frozen. Once solidified, the combustion port is made using a drill press. A general schematic of the fuel grain fabrication process can be viewed in Figure 6.

Safety

Safety measures are taken for every test. Once the stand is rolled to its right position outside, the wheels on the stand are chocked to ensure the stand will not roll during further setup or testing. No gas cylinders are moved and no valves are opened until the stand is stable. A fire extinguisher is placed beside the stand in case of a fire during testing. To ensure no faulty ignition, the spark plug is the last thing to be connected before firing. Traffic is stopped during each test to protect passing cars and people at approximately 50 yards distance. The flame is exhausted toward a dumpster in the case of damaging exhaust products. The start switch is located inside the building, and the operator also has ability to stop the test at any time by cutting off the oxygen supply. A roll up steel door is closed during testing and separates the operator from the test stand. The test is remotely viewed using a video camera outside connected to a television inside.

As seen in Figure 2, there are two check valves to prevent the reverse flow of gases in the propane line. One flash arrestor is used to stop any flame from coming back up the propane line. If a flame were to come back up through the line, the flash arrestor acts to snub out the flame. There have been no signs of reverse flow or flashes to date.

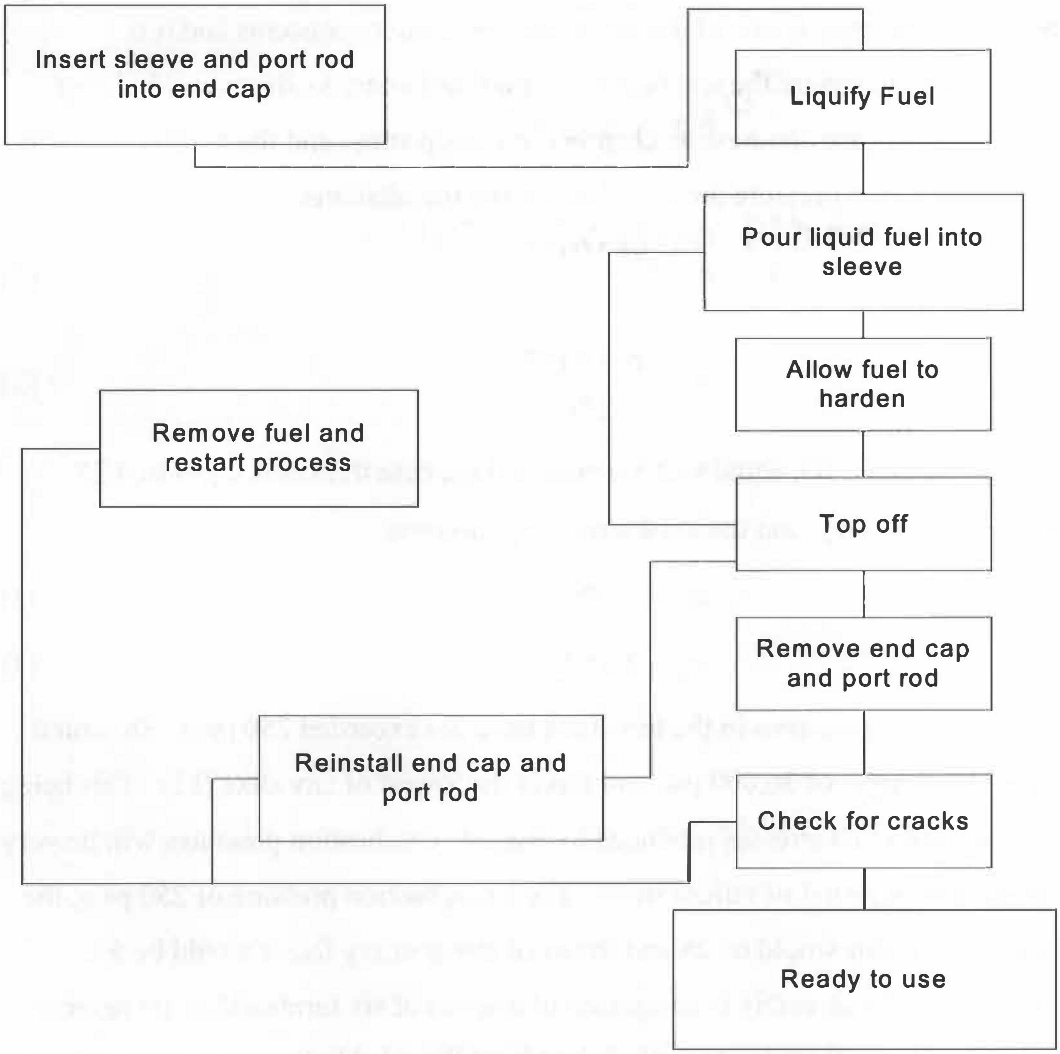

Figure 6: Grain Fabrication Schematic

Structural Analysis

Structural integrity is one of the more important safety concerns and it is considered in detail to ensure the test facility will not fail under loads imposed during testing. For the steel case combustion chamber, the hoop stress and the axial stress imposed by combustion pressure are calculated using the relations:

$$\sigma_h = \frac{P_c * ID/2}{t_s} \tag{1}$$

$$\sigma_a = \frac{P_c * ID/2}{2 * t_s} \tag{2}$$

With the inner diameter, ID, equal to 2.5 inches and the case thickness equal to 0.25 inches, the hoop stress, σ_h, and the axial stress, σ_a, become:

$$\sigma_h = 5 * P_c \tag{3}$$

$$\sigma_a = 2.5 * P_c \tag{4}$$

Combustion chamber pressures in the test stand have not exceeded 250 psig. Structural steel has a yield strength of 36,000 psi, and this is the lowest of any steel (13). This being stated, the hoop and axial stresses produced by feasible combustion pressures will be very small compared to any kind of failure stress. For a combustion pressure of 250 psig, the hoop stress safety factor would be 28 and the axial stress safety factor would be 57.

The turnbuckle assembly is comprised of a series of six turnbuckles, six reverse thread bolts, six reverse thread nuts, and six hex head threaded bolts. The nuts and bolts are steel while the turnbuckles are aluminum. The bolts are 0.25". The stress on the turnbuckle system is calculated as a straight bolt system using the relation:

$$\sigma_b = \frac{P_c * OD^2}{No_b * d_b^2} \tag{5}$$

or

$$\sigma_b = 24 * P_c \tag{6}$$

The bolt stress is greater than the case stress, but with given combustion pressures, bolt failure will not occur. For steel, a safety factor of 6 is calculated for combustion at 250 psig, and for aluminum, a safety factor of 4 is calculated for combustion of 250 psig.

However, failures have occasionally occurred on this system during preload. There is overloading on some parts of the turnbuckle system because no torque wrench is currently being employed in the tightening of the fuel grain into the test stand. The use of a torque wrench would essentially eliminate any overloading or overtightening of the bolts.

Test Procedure

The stand is rolled onto a loading dock with the exhaust end facing away from the building and the wheels are chocked. The fuel is weighed, inserted, and preloaded. The case is tightened using a star pattern so that overloading on 1 bolt or screw is less likely to occur. The instrumentation is simultaneously set up and checked to be working properly by collecting data and viewing the data using the real time output on the HP VEE program screen. Once the instrumentation is verified to be working properly and the fuel grain is locked in place, the oxygen and propane lines are charged to the desired supply pressure for the test. After this is completed, all tools and other equipment not in use are removed from the stand. The strain gage is then calibrated. After this is completed, the traffic is stopped, the HP VEE program is started, a camera is set to record the test, and the spark plug is attached. The loading dock bay door is closed after this, and the test is ready to begin. The test is started using a control panel with a switch having two positions, safe and armed, and a fire button. The switch is turned to armed, and the fire button is pressed. The test can be shut off at any time by turning the switch back to safe. After the test, the spark plug is removed and the collected data is saved to the computer. The oxygen and propane lines are then discharged. The fuel grain is then removed, and a final mass is taken. The stand and other equipment are stored inside once all grains have been fired for the day. With no delays, a complete test can be performed in around 30 minutes.

Test Summary

Testing began in the fall of 2003 and was completed for purposes of this thesis in the summer of 2005. Fuels successfully tested for the purposes of this research include lard soaked in a sponge matrix and beeswax. Lard without a matrix was tested once, but was unsuccessful due to solid droplets of lard, some up to the size of a dime, being blown out of the engine unburned. It was assumed lard itself was not strong enough to resist the shear force exerted on it by a low oxygen flow, so it was not tested again. This being stated, lard was mixed with a proven fuel, paraffin, and also inserted into a sponge matrix to increase stability. Both methods have proved successful. The lard/paraffin fuel mixture was tested mostly prior to work done for the purposes of this thesis and only at lower combustion pressures. The majority of tests for this thesis have used beeswax as the fuel.

There were unsuccessful tests with each type of fuel, but these failures were not usually attributed to problems with the fuel itself. The only known fuel failure is when a grain collapses on itself creating a new port curving around the top of the grain. This is noticed after the test. With this type of failure it should be noted that the test is still functional and data is still collected. This collapsing of the grain failure has only occurred a handful of times. The data was not used in analysis considering the difference in conditions.

The remaining failures are classified into instrumentation and hardware failures. Looking at the instrumentation failures, these tests typically occur when the data collection system did not work properly. It is assumed that some crossed wires of different voltages caused errors in data output on a few tests. Another major problem was the data acquisition card. With the insertion and removal of this card after each day of tests, it wore the input multiplexor to where the computer would not even recognize the card. This was not determined until the card was sent to the manufacturer and repaired. With the fixed card and a complete rearrangement of the wiring, the instrumentation failures were greatly reduced.

As for the hardware failures, there are a couple of notable cases. When the chamber is not tightened into the assembly correctly, liquefied fuel can leak out through the end caps during the test. This could be due to either (a) not tightening enough or (b) unequal loading on bolts. Both of these cases have occurred at some point. As for the tightening issues, they do not occur often. The bolt assembly is tightened and checked by another person. With the use of a torque wrench, case (b) could be all but eliminated.

Other failures arose due to different size cases and injector end cap problems. The failure due to the different size cases was quickly remedied. After this problem was fixed, failures at the injector end cap were occurring with the flame acting as a torch and cutting into or through the steel cap. It was soon noticed that the failures were being caused by a flow problem. The oxygen was being supplied at a much greater area than the initial fuel port area, at an area ratio of 9. This allowed the oxygen to hit flush on the end of the fuel grain as well as flow over it. When the flow hit the top of the fuel grain it pushed itself out through the fore end of the combustion chamber. To solve this problem, a 0.25 inch thick, stainless steel restrictor plate was made to get the flow down to a smaller area. This effect can be seen in Figure 7. The fuel grain now meets this plate flush. No hardware problems have since occurred. In addition to this, the bottom of the grain has been left open so at the aft end of the chamber a more complete combustion is allowed to occur. This 0.5" gap at the end is considered the mixing chamber and accounts for 5% of the chamber length.

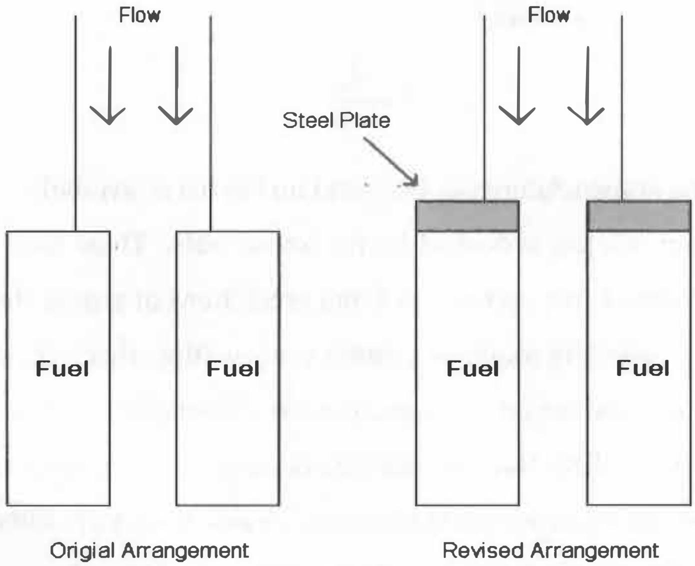

Figure 7: Before and After Restrictor Plate

III. TEST ANALYSIS AND RESULTS

Data Analysis

For each test, pressure data just upstream and downstream of the orifice plate, and strain data is collected. The initial and final masses of the fuel grains are also measured. The thrust is calculated using the linearly fitted calibration curve. The calibration is checked prior to each test to ensure a near unity correlation coefficient is reached. The two measured pressures are used to determine the average oxygen flow rate. The downstream pressure of the orifice plate is taken to be the combustion pressure.

The regression rate of a fuel is the rate at which the fuel is consumed, and is taken as distance normal to the surface consumed in a given time. The average regression rate is simply taken to be the change in radial grain thickness divided by the time of the burn. This is shown below. The final thickness of the grain is found using the final mass of the fuel, the density of the fuel, and the volume (known case dimensions). Data reduction details can be found in Appendix C.

$$\dot{r} = \frac{t_{g_f} - t_{g_i}}{t_b} \tag{7}$$

Clarification on the nomenclature can be found on the list of symbols.

A regression rate law is desired for the tested fuels. These laws are useful in allowing comparisons of fuel performance and predictions of engine thrust profiles. These relations are generally found as a function of oxidizer flux rate, propellant flux rate, grain length, or combustion pressure, or some combination of these parameters. The most common is the oxidizer flux rate and this is simply the average oxidizer flow rate divided by the average cross-sectional port area. A power curve is fitted to the data to find the relation. The simplest of these relations takes the form of

$$\dot{r} = a * G_{ox}^{\ n} \tag{8}$$

The total impulse imparted is found from the integrated thrust over time. A basic Riemann squares approximation is used to determine the impulse between each time increment, and these are summed over the duration of the test to find the total impulse. With knowledge of the total impulse and the consumed propellant mass, the exit velocity and specific impulse can be easily determined. For ideal expansion (that is, exit pressure is equal to ambient pressure), exit velocity is simply the total impulse divided by the consumed propellant mass, and the specific impulse is the exit velocity divided by the gravitational constant, 9.81 m/sec^2. The specific impulse is an important parameter of not only hybrid rocket performance, but in general rocketry as well. It is the theoretical thrust from an equivalent rocket that has a propellant weight flow rate of unity.

$$I_{sp} = \frac{\sum_{i=0}^{i=t_b} \frac{1}{2}(T_{i+\Delta t} + T_i) * (t_{i+\Delta t} - t_i)}{g * m_{prop}} \tag{9}$$

The equivalence ratio is useful to determine if the combustion is operating in a fuel-rich or fuel-lean state. It is simply the ratio of the oxidizer to fuel ratio to the stoichiometric ratio, or

$$\phi = \frac{{}^{O}\!/_{F}}{\left({}^{O}\!/_{F}\right)_{stoich}} \tag{10}$$

The equivalence ratio plays a large factor in performance of the vehicle. For equivalence ratios less than unity, the combustion is fuel-rich, and if higher than unity, the combustion is fuel-lean. If operating well outside of unity, then performance can be greatly decreased. Also, the peak value of many parameters, i.e. temperature or specific impulse, do not necessarily occur at an equivalence ratio of unity. Figure 8 shows these general principles in relation to the specific impulse for both shifting equilibrium and frozen flow assumptions for both beeswax and lard with oxygen combustion at 150 psig (14). These calculations are for theoretical conditions, that is, the flow is ideally expanded. Shifting equilibrium assumes that chemical reactions can take place as the flow moves through the nozzle, while frozen flow assumes no chemical reactions take place as the flow moves through the nozzle. Figure 9 shows the molecular weight of the combustion products versus equivalence ratio, and Figure 10 shows the relation of combustion temperature to equivalence ratio. The stoichiometric oxidizer to fuel mass ratio for these calculations is 3.3 for beeswax with oxygen, and 2 for pure lard with oxygen. The thermodynamics code used to calculate theoretical parameters is a United States Air Force code (15).

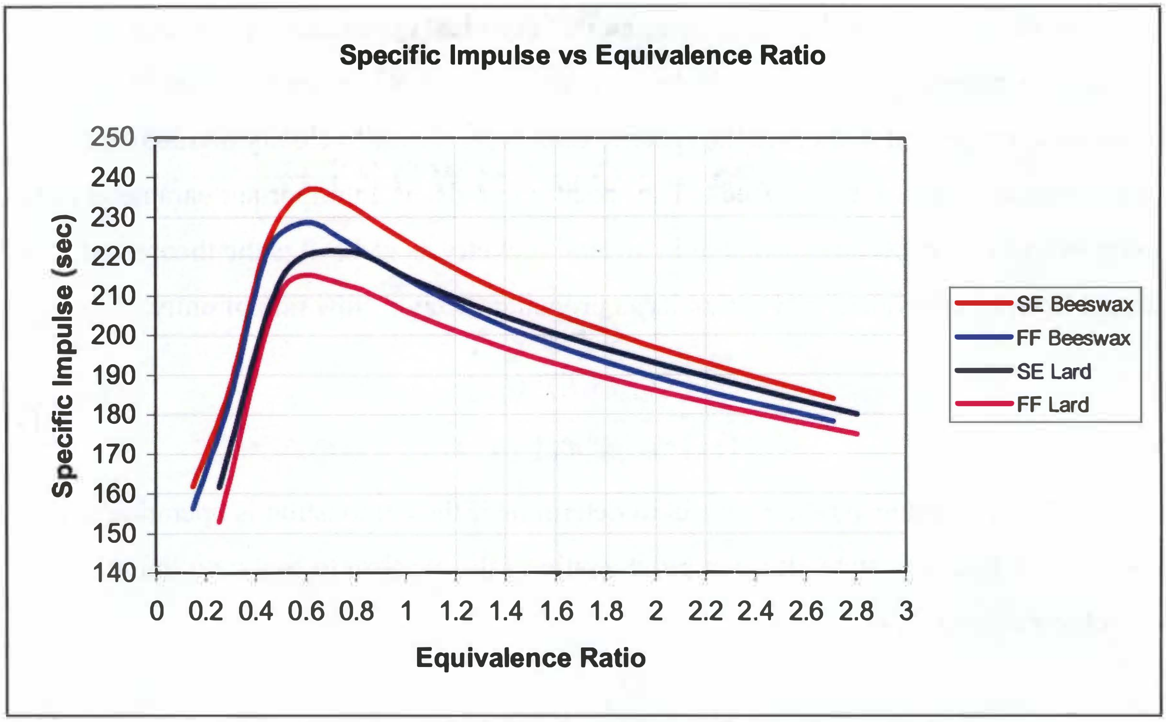

Figure 8: Theoretical Sea Level I_{sp} vs. Equivalence Ratio

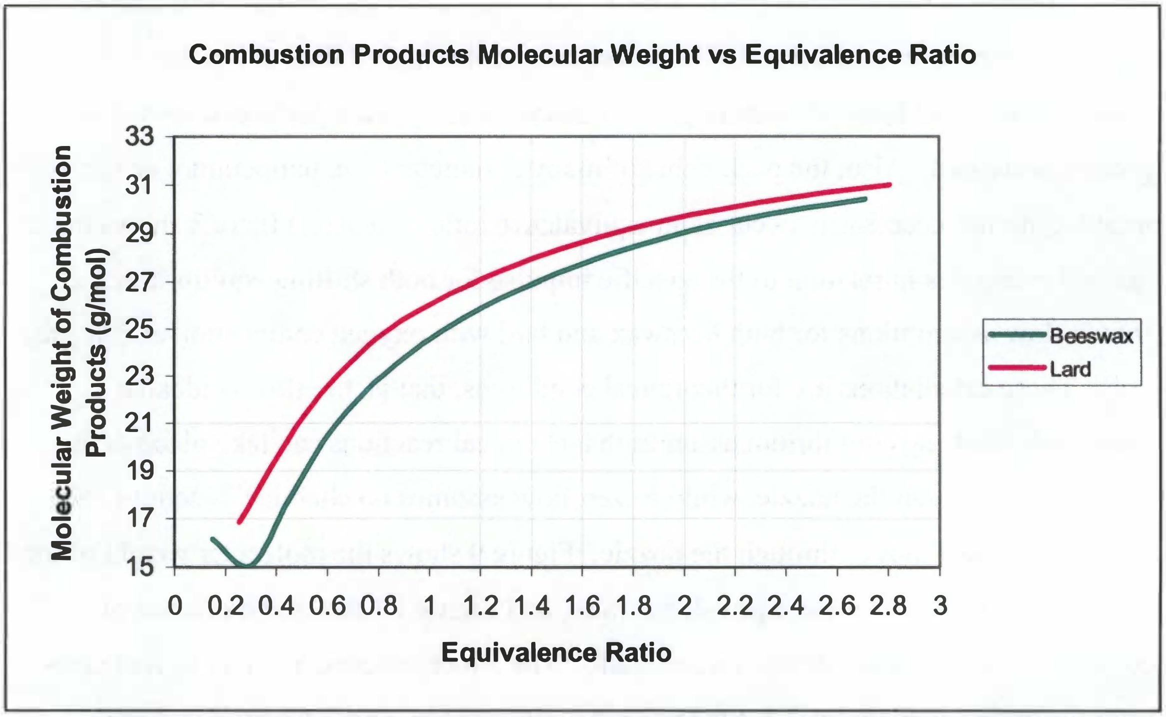

Figure 9: Theoretical Products Molecular Weight vs. Equivalence Ratio

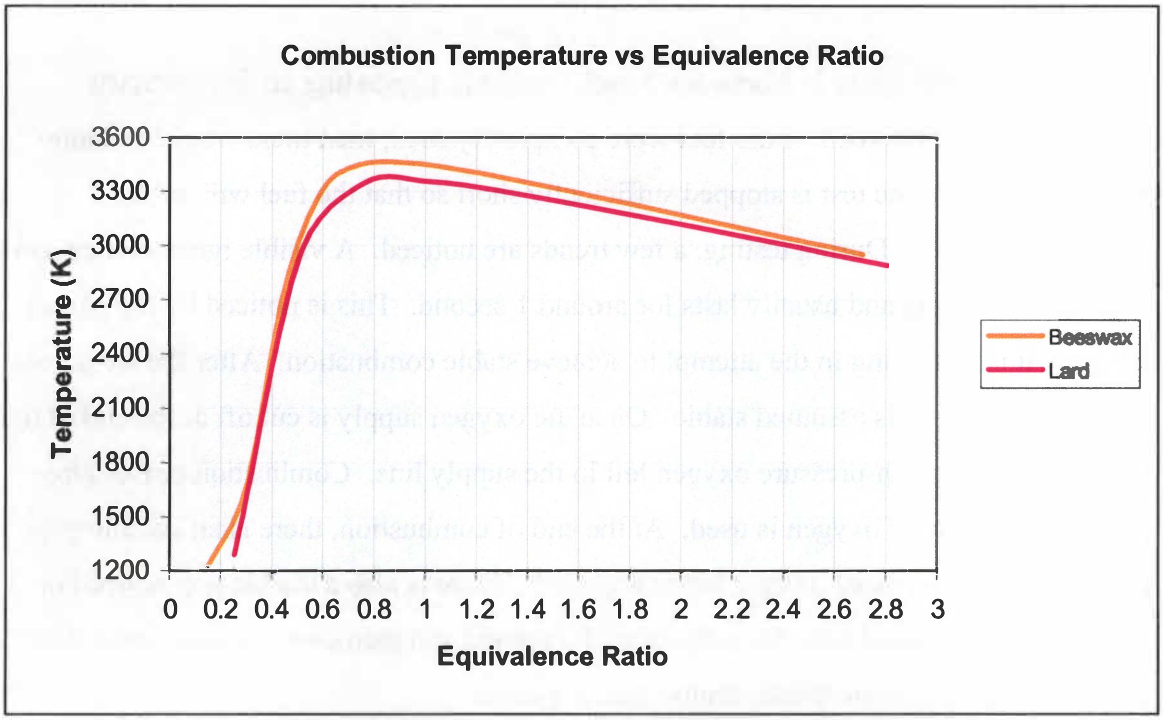

Figure 10: Theoretical Combustion Temperature vs. Equivalence Ratio

As noticed, the highest specific impulse is at an equivalence ratio around 0.65. The highest value of specific impulse is not located at the stoichiometric equivalence ratio because of dissociation in the products of combustion. Deviating to a further fuel rich mixture greatly decreases the specific impulse while deviating towards a fuel lean mixture decrease the specific impulse as well but at a slower rate. With a fuel rich mixture, there is incomplete combustion, thus a decreasing trend in the molecular mass of the combustion products. The combustion temperature also decreases, and at a much faster rate than the molecular mass of the combustion products. This being said, vacuum specific impulse and sea level specific impulse will both decrease.

$$I_{sp_{vac}} = \sqrt{\frac{2(\gamma+1)}{\gamma} \frac{R_u * T_c}{\mu}} \tag{11}$$

For fuel lean mixtures, the molecular weight of the combustion products increases slightly while combustion temperature decreases slightly. This yields a decreasing specific impulse, but at a slower rate than excessively fuel-rich mixtures.

Test Trends

Each test is set to last between 5 and 7 seconds, depending on the predicted characteristics of the fuel. If the fuel were completely used, then there would be faulty data at the end, so the test is stopped sufficiently short so that the fuel will not be completely burned. During testing, a few trends are noticed. A visible ignition transient is generally present and usually lasts for around 1 second. This is noticed by the plume and how it is sputtering in the attempt to achieve stable combustion. After the sputtering ceases, combustion is assumed stable. Once the oxygen supply is cut off at the end of the test, there is still high-pressure oxygen left in the supply line. Combustion ceases after this small amount of oxygen is used. At the end of combustion, there is an audible pop because there is no more oxygen being supplied. There is also a visible pop noticed in the plume as it grows larger for a fraction of a second and then ceases completely. This is nothing more than the thrust termination sequence.

There are also some general trends to note in the collected data. First, an ignition transient is noticed by the noise at the start of the burn in many tests. This sputtering corresponds to the aforementioned viewed ignition. Also the peak values of the pressure and thrust are located directly after combustion becomes stable, that is, right after the ignition transient. After these peaks there is a slight decline in data values throughout the test until the oxygen supply is cut off. When cut off, the pressure and thrust return to their 0 values. These trends will be noticeable in Figures 11-13. Approximately 200-300 grams of fuel is burned during each test.

Data Results

Typical data curves are presented in Figures 11-13. These curves are for Test 34, dated June 7, 2005, and are representative of other tests. In this test, oxygen was supplied at 400 psig, and the test was run for 5.5 seconds with a 0.7 sec shot of propane at the start. Beeswax was the fuel. The thrust versus time is presented in Figure 11, the combustion pressure versus time is presented in Figure 12, and lastly, Figure 13 shows the pressure difference across the orifice plate.

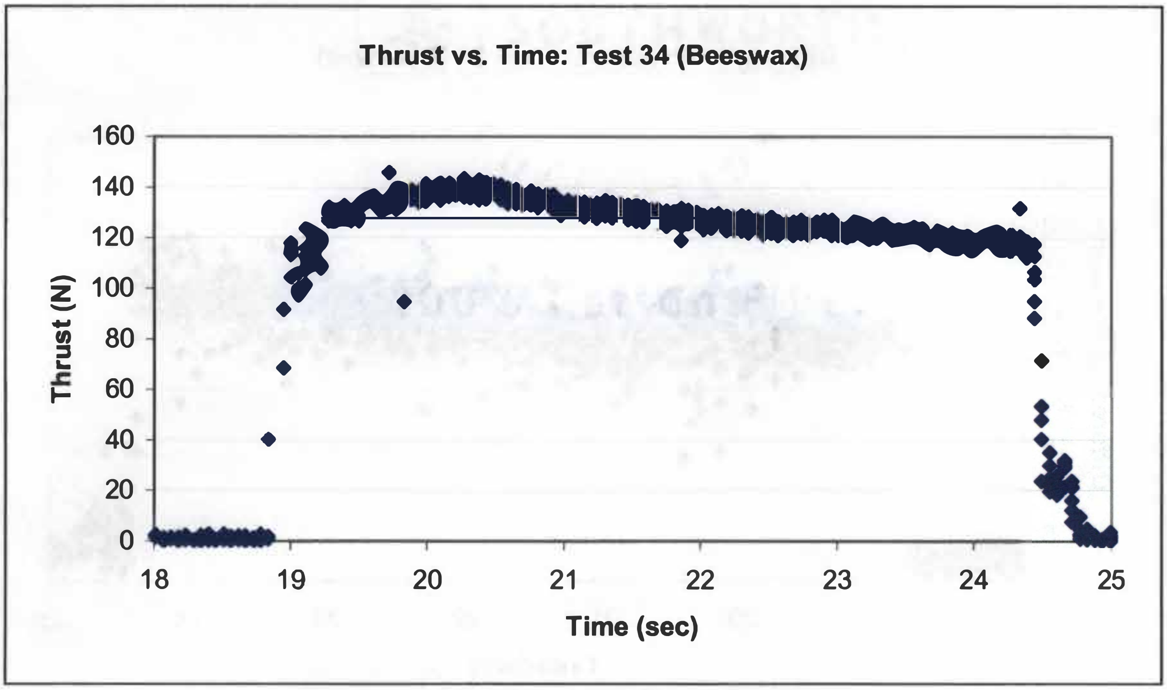

Figure 11: Thrust vs. Time (Test 34)

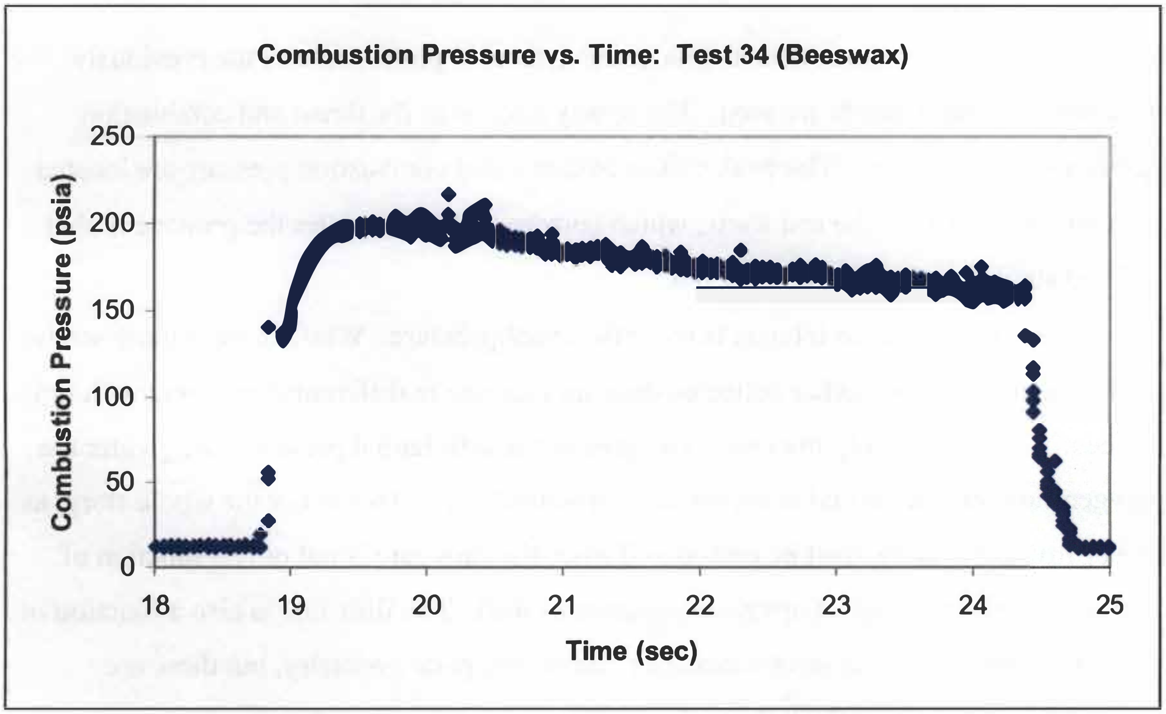

Figure 12: Combustion Pressure vs. Time (Test 34)

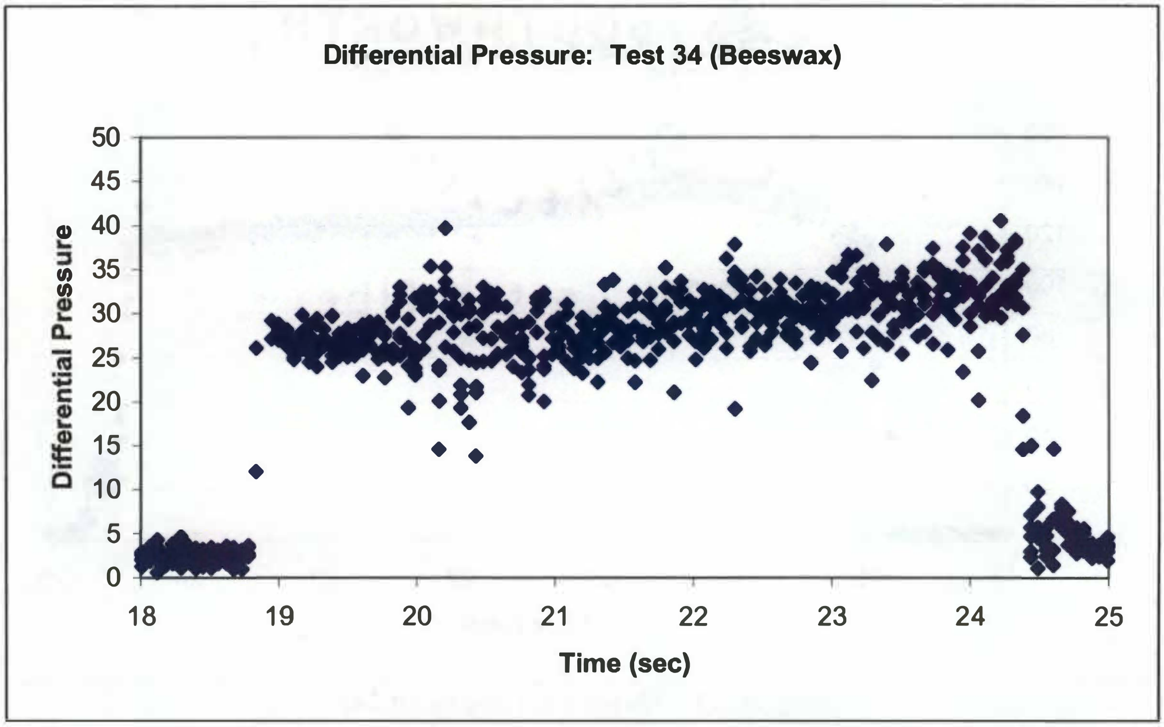

Figure 13: Orifice Pressure Drop vs. Time (Test 34)

In looking at the collected data in the presented plots, some of the previously mentioned general trends are seen. The steady decline in the thrust and combustion pressure values is clear. The peak values of thrust and combustion pressure are located around a second after the test starts, which corresponds to just after the propane is shut off and stable combustion is achieved.

One parameter of interest is the differential pressure. While there is more scatter with this data than any other collected data, an increase in differential pressure with time is seen. This is generally the case. The greater the differential pressure, the greater the oxygen flow rate, as would seem the case presented here. This is not the whole story, as the upstream pressure must be considered since the flow rate is not only a function of differential pressure but of upstream pressure as well. The flow rate is also a function of other parameters such as gas temperature and orifice plate geometry, but these are assumed constant throughout the test.

$$\dot{m}_{ox} = \frac{e * C * A_t * \sqrt{(2 * \rho * \Delta P)}}{\sqrt{(1-\beta^4)}} \tag{12}$$

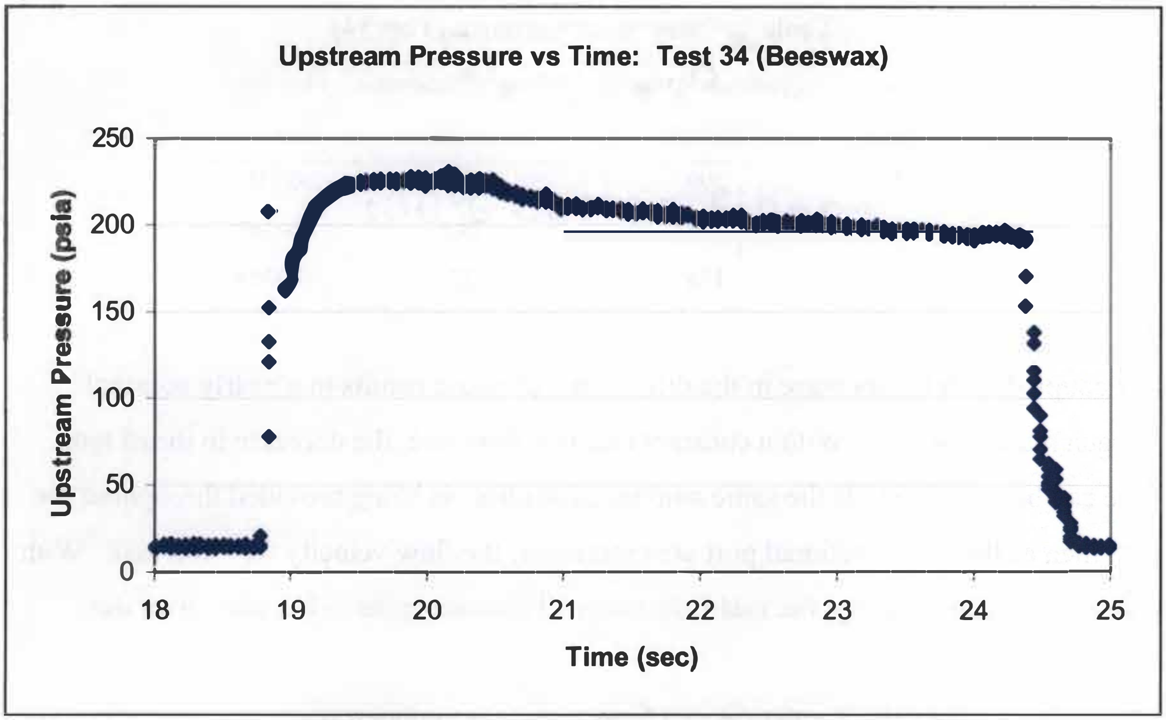

Figure 14: Upstream Pressure vs. Time (Test 34)

The upstream pressure versus time data can be seen in Figure 14. The regressive trend noticed in this data is typical and is assumed to be caused by pressure loss variations with time through the gas lines and through the orifice in the solenoid valve. This data is used to calculate the average oxidizer mass flow rate.

Considering an increase in average pressure differential throughout the test coupled with a decrease in average upstream pressure, the change in the calculated oxygen flow rate is minimal. This is found to be the case upon analyzing three data points in a test with one near the start, one in the middle, and one near the end of the test. Looking specifically at Test 34, the differential data is first linearly fitted and used to find the differential pressure at a given time. Taking these differential values with the corresponding upstream pressure values, the flow rate is calculated using the same MATLAB code used to calculate the average flow rate. The results are presented in Table 1.

The flow rate remains nearly constant based on these calculations. This result has been found in three other tests, so it is assumed that the oxygen flow rate has minimal change throughout all tests. This implies that the decrease in the upstream pressure during the

Table 1: Flow Rate Variance (Test 34)

Time (sec)	Upstream Pressure (psig)	Pressure Difference (psig)	Flow Rate (kg/sec)
20	209	27	0.039
22	188	29.5	0.0383
24	178	32	0.0384

test coupled with the increase in the differential pressure results in a nearly constant oxygen mass flow rate. With a constant oxidizer flow rate, the decrease in thrust with time can be explained. If the same amount of oxidizer is being provided throughout the test, then as the cross sectional port area increases, the flow velocity will decrease. With a decreased flow velocity, the fuel flow rate will also decrease. This will lower the thrust.

One of the main results desired from testing is to obtain regression rate data. The regression rate versus oxidizer flux rate is presented in Figure 15 for both beeswax and lard in a sponge. Also shown are regression rate characteristics for the common hybrid rocket fuel, HTPB, using the regression rate law from Sutton (2) and the paraffin regression rate law from Stanford/NASA Ames (3). All tests used gaseous oxygen as the oxidizer for valid comparison.

$$\text{HTPB: } \dot{r} = 0.146 * G_{ox}^{0.681} \tag{13}$$

$$\text{Paraffin: } \dot{r} = 0.488 * G_{ox}^{0.62} \tag{14}$$

There is sufficient scatter in the experimental data to prevent the formation of a regression rate equation for either beeswax or lard. The scatter is assumed to be caused from errors in collected data as well as variations in grain structure caused by air pockets in the fuel. It is noticed though that every regression rate in the tested oxygen flux range is at least 3 times as great as that of HTPB for both fuels. Also, the regression rate is similar to or greater than that of paraffin for similar flux rates. These results confirm that the tested fuels exhibit the desired high regression rates. This is encouraging since that high regression rates lead to decreased structural needs for a theoretical rocket, thus decreasing the inert mass fraction. It is hypothesized that the reason for the increased regression rate lies in the increased surface area created in the same liquid surface of the

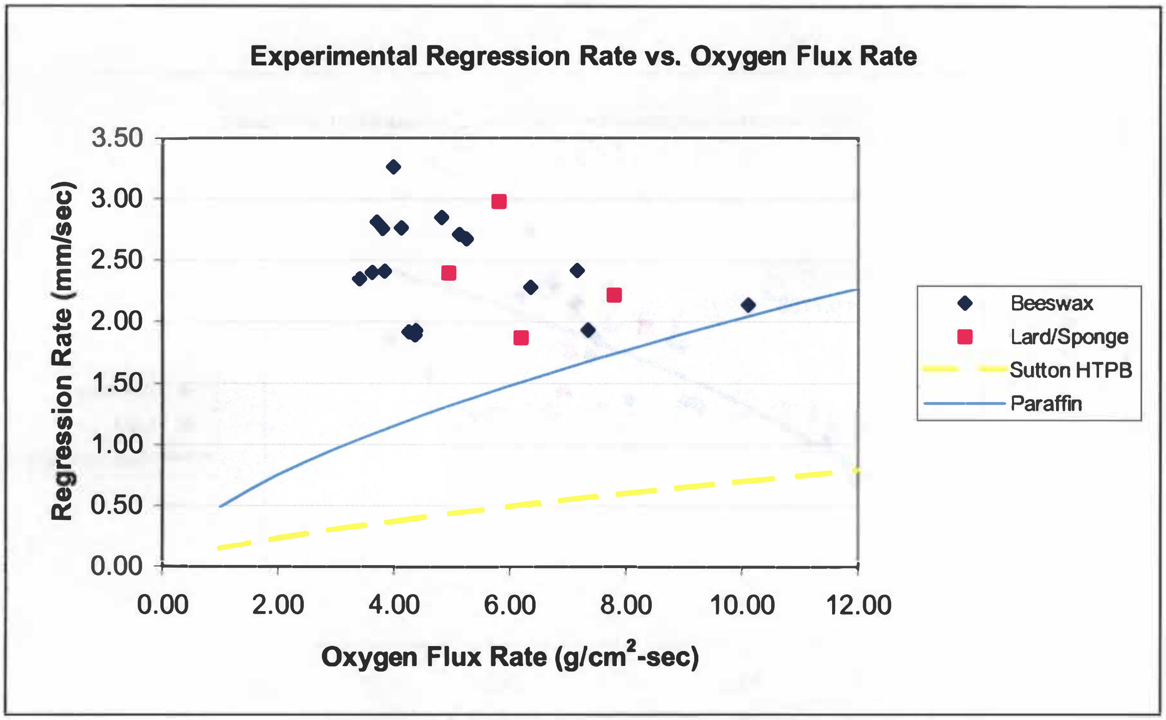

Figure 15: Regression Rate vs. Oxidizer Flux

fuel as mentioned with the paraffin. The fuels used in this research offer a higher rate of fuel mass transfer than paraffin, and therefore, a higher regression rate.

The experimental regression rate versus combustion pressure is presented in Figure 16. No data is shown for previously tested fuels, as regression rate laws as a function of combustion pressure are not typically determined for hybrid rockets. Regression rates as a function of combustion pressure are common for solid propellant because the burning takes place on the surface instead of inside a boundary layer caused by oxidizer flow like in hybrids. This is not to say that regression rate as a function of combustion pressure is not viable in hybrids, but it is not typically determined.

A general trend of increasing regression rate with combustion pressure is seen for beeswax. There are no trends noticed in the lard/sponge data due to the low number of tests. For the tests analyzed, there is a better correlation between regression rate and combustion pressure than with oxidizer flux rate. Hybrid fuels are known to be essentially dependent upon oxidizer flux rates, so this is an interesting result. A rough regression rate law versus combustion pressure for beeswax is given below.

$$\dot{r} = 0.1995 * P_c^{0.4891} \quad (15)$$

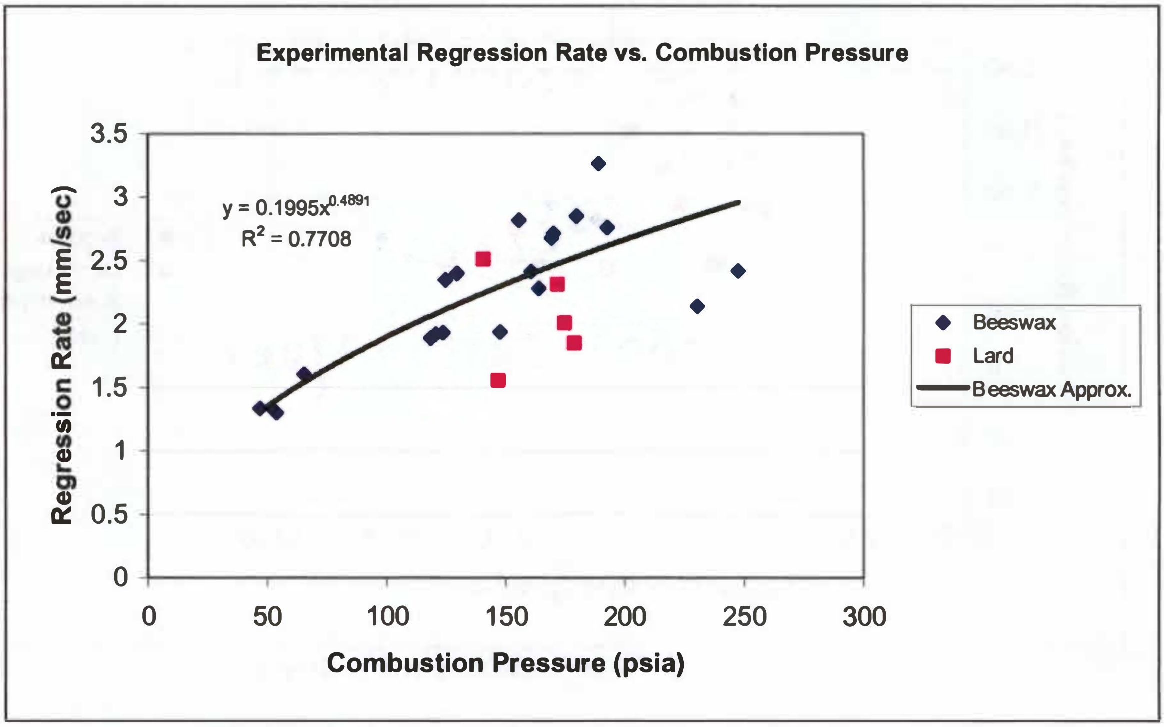

Figure 16: Regression Rate vs. Combustion Pressure

All tests resulted in fuel rich mixtures. Some characteristics to note involve the equivalence ratio and its relation to other parameters. Figures 17 and 18 show the specific impulse and combustion pressure as a function of equivalence ratio. The specific impulse is corrected for off ideal conditions, that is, the pressure thrust has been removed in the calculation. Both nozzle geometries are presented, with C corresponding to the converging only nozzle, and CD corresponding to the converging-diverging nozzle.

In comparison to theoretical performance (Figure 8), it is noted that nearly every value is below theoretical performance values. These values were corrected for off ideal conditions, so comparison of every point to theoretical value is valid. Resulting errors are assumed to partly arise from the approximation of specific impulse.

There is significant scatter in the combustion pressure data, so analysis is limited and difficult. However, from Figure 18 it appears that combustion pressure slightly increases with equivalence ratio. If this argument is correct, then it implies that the oxygen flow rate is increasing more rapidly than the fuel flow rate as combustion pressure increases. Performance would be greatly enhanced if the equivalence

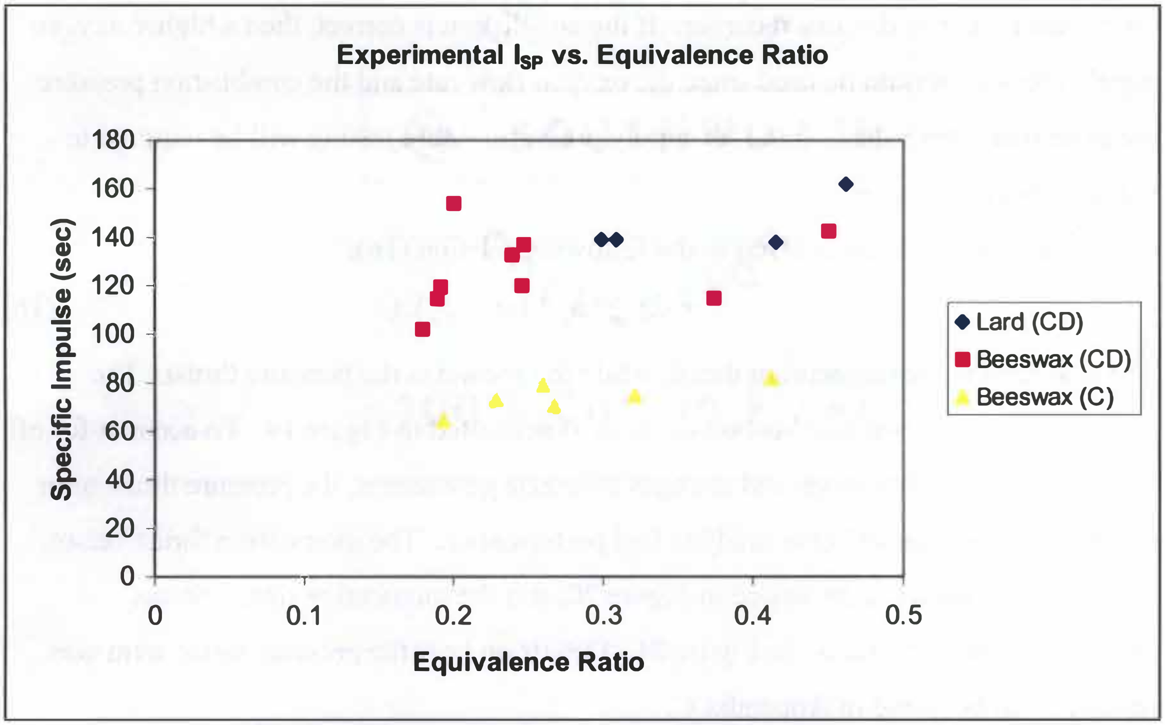

Figure 17: Specific Impulse vs. Equivalence Ratio

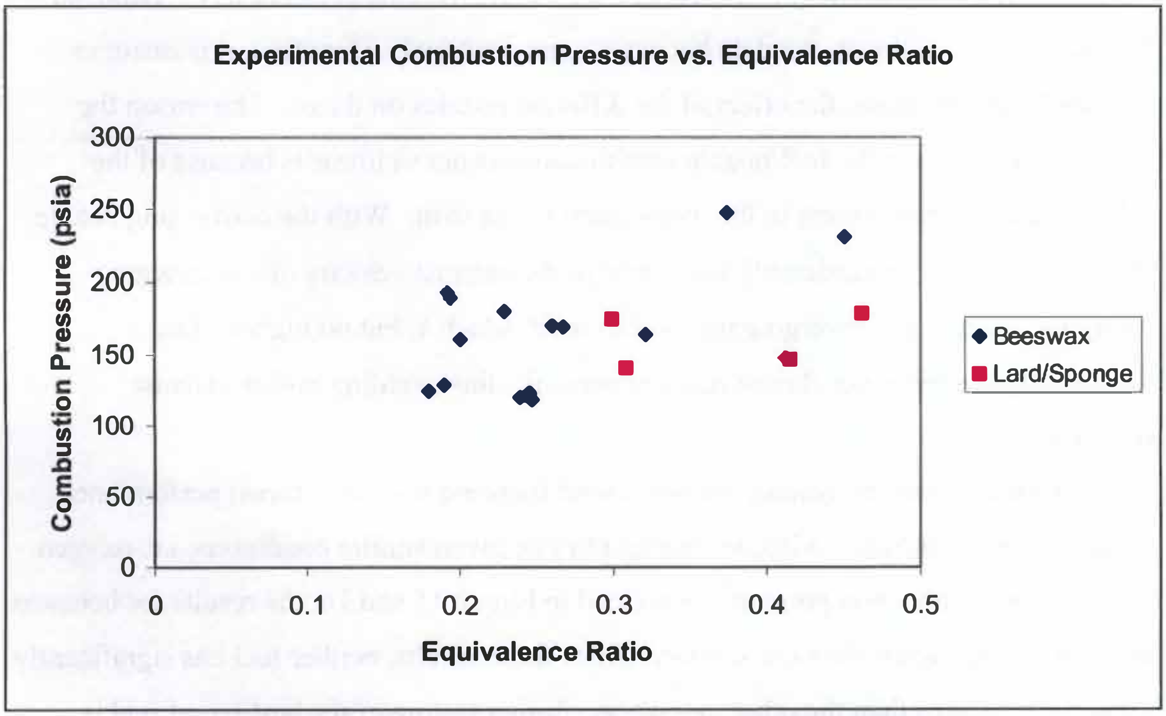

Figure 18: Combustion Pressure vs. Equivalence Ratio

ratio were higher as discussed earlier. If the conclusion is correct, then a higher oxygen supply pressure should be used since the oxygen flow rate and the combustion pressure are essentially dependent on the set supply pressure. More testing will be required to validate this conclusion.

A rocket's thrust is given in the following relation (16):

$$T = \dot{m}_{prop} * u_e + (p_e - p_a)A_e \tag{16}$$

The first term is the momentum thrust, while the second is the pressure thrust. The measured thrust versus combustion pressure is presented in Figure 19. To account for off ideal combustion conditions and changes in nozzle geometries, the pressure thrust term ought to be removed to better analyze fuel performance. The momentum thrust versus combustion pressure is presented in Figure 20, and the momentum thrust versus propellant flow rate follows in Figure 21. Details on how the pressure thrust term was removed can be found in Appendix C.

As seen in Figure 19, the measured thrust for both fuels and nozzle geometry conditions produces a nearly linear result. However, with the pressure thrust removed from the measured thrust, the data becomes more scattered. Therefore, it is easier in Figures 20 and 21 to see the effect of the different nozzles on thrust. The reason the momentum thrust for the fuel/nozzle combinations is not as linear is because of the exhaust velocity component in the momentum thrust term. With the converging nozzle, this value drops off considerably compared to the exhaust velocity of a converging-diverging nozzle. A converging nozzle can reach Mach 1, but no higher. The converging-diverging nozzle can reach supersonic, thus yielding higher exhaust velocities.

Based on current results, the two tested fuels are similar in thrust performance given similar conditions. Also, for regression rate given similar conditions, i.e. oxygen flux rate and combustion pressure, as noticed in Figure 15 and 16, the results for beeswax and lard in a sponge matrix are similar. Given these results, neither fuel has significantly better performance than the other. However, further testing of the lard-based fuel is warranted to provide a more complete data set.

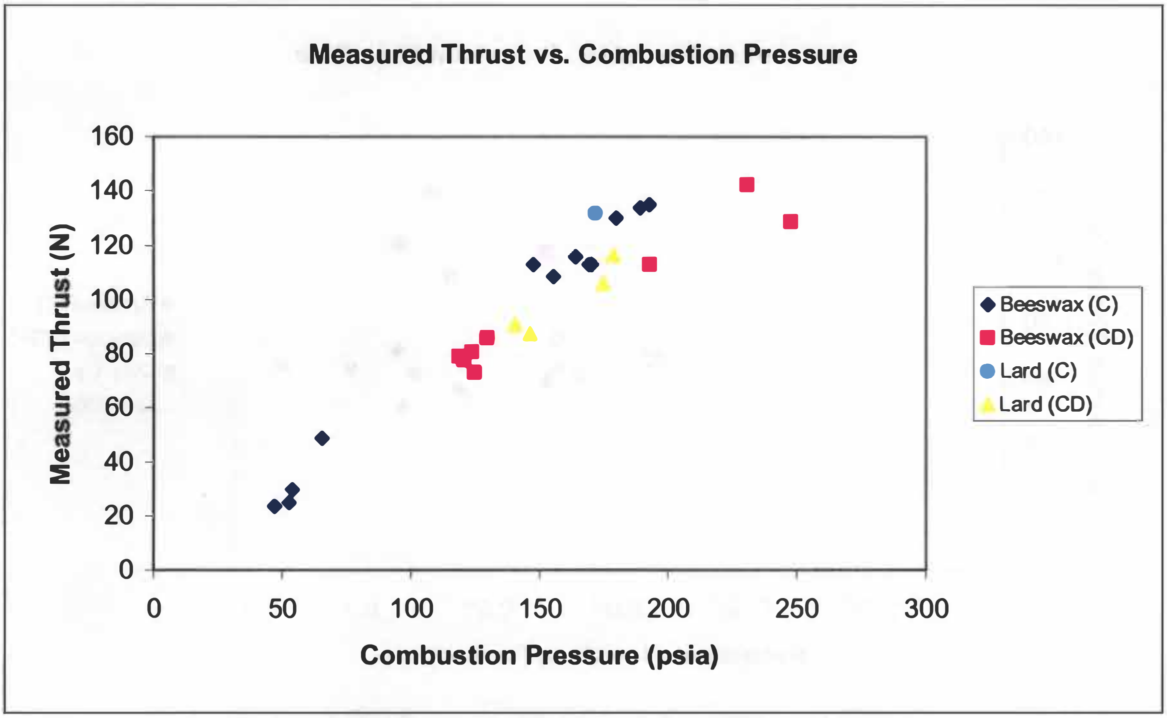

Figure 19: Measured Thrust vs. Combustion Pressure

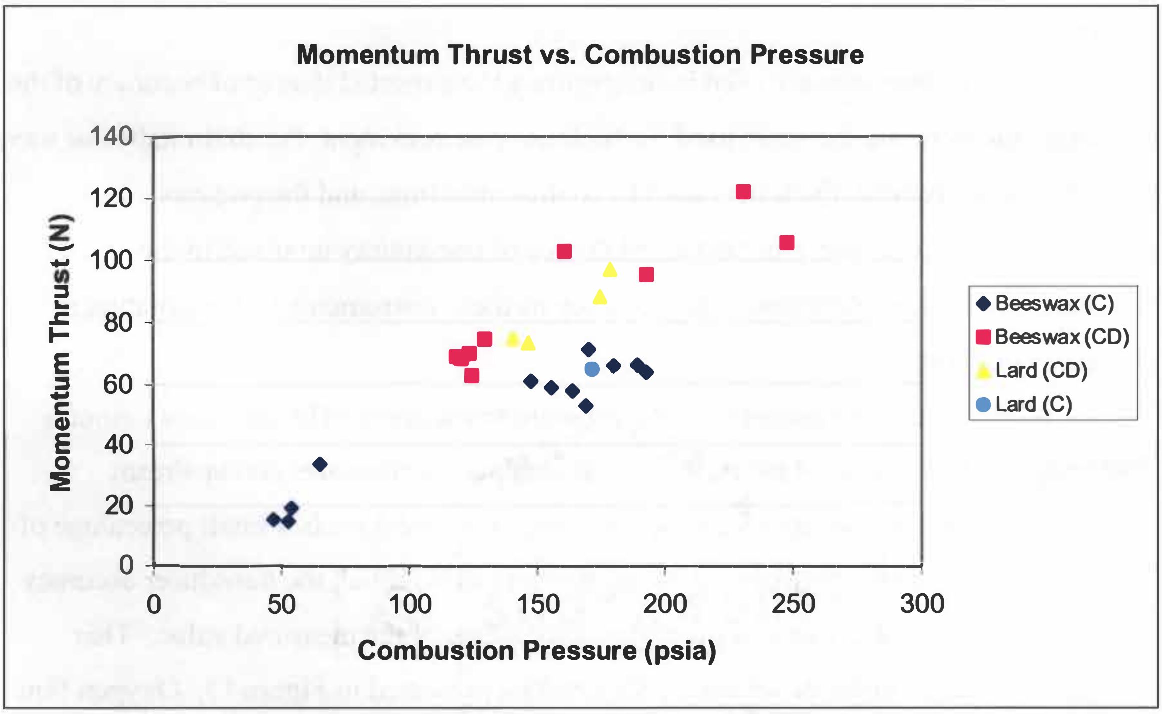

Figure 20: Momentum Thrust vs. Combustion Pressure

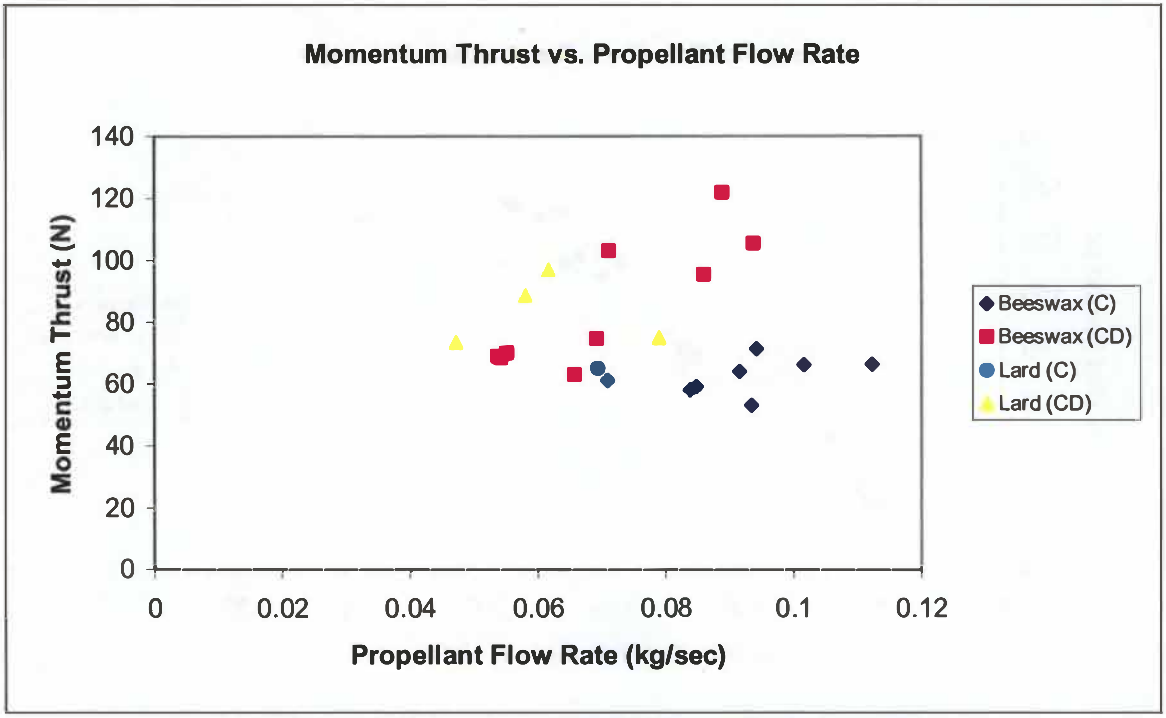

Figure 21: Momentum Thrust vs. Propellant Flow Rate

Uncertainty

A few instruments are used in determining the expected degree of accuracy of the research. Included are the scale used for fuel mass measurement, the strain indicator used for thrust measurement, the timers used to control burn time, and the pressure transducers. There is also some expected degree of uncertainty involved in the calculation of oxygen flow rate. The accuracy of these instruments and calculation is presented in Table 2.

Worth note is the accuracy of the pressure transducers. The full-scale output is 1000 psig, so +/-0.4% is a 4 psi swing. With combustion pressures and upstream pressures, this value does not affect the data much because 4 psi is a small percentage of the measured pressure. However, with the pressure differential, the transducer accuracy is much more evident because of the higher percentage of the measured value. This explains the scatter in the differential pressure data presented in Figure 13. Oxygen flow rate data is calculated using a constant temperature assumption of 75 °F. As noticed, there is a 2.3% change in differing the gas temperature by 25 °F.

Table 2: Instrument and Calculation Accuracy

Instrument	
Scale	1 gram resolution
	Accuracy From Manufacturer (+/- %)
Strain Indicator	0.1 (full scale)
Timers	1 (set value)
Pressure Transducers	0.4 (full scale)
GOX Flow Rate Uncertainty	Accuracy (+/- %)
Due To Temperature Variations	2.3 @ +/-25 °F

IV. CONCLUSIONS AND RECOMMENDATIONS

Two fuels, lard in a sponge matrix and beeswax, for use in hybrid rocket motors have been successfully tested in a laboratory scale combustion chamber. Both fuels have displayed the desired high regression rates, thus overcoming one of the major shortcomings of general hybrid rocket fuels. These fuels have shown regression characteristics three to four times that of HTPB, and are similar or greater than those of paraffin-based fuels. A rough law for regression rate as a function of chamber pressure was achieved for beeswax, and the specific impulse relation to equivalence ratio was analyzed.

With the testing success of these fuels, more tests using these fuels are planned. It is also desirable to test other potential fuels such as partially hydrogenated coconut oil. Pure lard may be possible to test again without the use of a stabilizing agent such as paraffin or a mechanical matrix. This is thought possible because at higher flow conditions, the fuel would be allowed to burn to completion more so than at low flow conditions.

It is recommended that testing should occur in a greater range of oxidizer flux rates and that testing should also occur at higher equivalence ratios to harness the current unused energy. With the increased flux rates, better comparisons of regression rate characteristics could be made with other fuels. With an increased equivalence ratio, a performance increase would be achieved because of increases in various parameters such as combustion temperature and specific impulse. The low equivalence ratios are assumed to be caused by the short mixing chamber. Typical length to diameter ratios range from 0.5-1, and the current ratio is 0.2.

It is possible that noise is disturbing the data collection. A 60 Hz signal is thought possible, and checks against this should be made. Also, to lessen the scatter in the data, a better way of fabricating fuel grains is recommended so as to remove any air pockets formed. These air pockets, when uncovered during a test, create more surface area instantaneously, thus changing some parameters including regression rate and oxidizer flux rate.

Overall, the testing of these fuels is considered a success. Both lard in a sponge matrix and beeswax have demonstrated the desired results of being a biologically derived, non-toxic, non-hazardous fuel with a high regression rate when compared to conventional fuels.

REFERENCES

1. Humble, R.W., Henry, G. N., Larson, W.J. *Space Propulsion Analysis and Design*, 1st ed., The McGraw-Hill Companies, Inc. (1995).
2. Sutton, G. P., *Rocket Propulsion Elements: An Introduction to the Engineering of Rockets*, 6th ed., John Wiley and Sons, New York (1992).
3. Karabeyoglu, M.A., Cantwell, B.J., Altman, D. Development and Testing of Paraffin-Based Hybrid Rocket Fuels. AIAA Paper 2001-4503.
4. Karabeyoglu, M.A., Zilliac, G., Cantwell, B.J., De Zilwa, S., Castelluci, P. Scale-Up Tests of High Regression Rate Liquefying Hybrid Rocket Fuels. AIAA Paper 2003-1162.
5. Wikipedia. *Hybrid Rockets*. http://en.wikipedia.org/wiki/Hybrid_rocket.
6. Covarrunias, Amanda. Toxin Found in Simi Valley's Ground Water, *The Los Angeles Times*, December 5, 2002.
7. The Associated Press, Fuel Chemical Tainting Some Groundwater, *The Salt Lake Tribune*, January 7, 2003.
8. The Environmental Working Group. *Rocket Science, Chapter 3*. http://www.ewg.org/reports/rocketscience/chap3.html.
9. Environmental Protection Agency. http://www.epa.gov/swerffrr/documents/perchlorate/htm.
10. LMNO Engineering, Research, and Software, Ltd. Ohio, USA. http://www.lmnoeng.com/flow/smallorificegas.htm.
11. Grant, D.L. Beeswax. Bureau of Chemical Safety. Ottawa, Ontario, Canada. http://www.inchem.org/documents/jecfa/jecmono/v30je11.htm.
12. Moyna, Guillermo. http://tonga.usip.edu/gmoyna/biochem341/lecture28.html. (1999).
13. Riley, William F., Sturges, Leroy D., Morris, Don H. *Mechanics of Materials*, 5th ed., John Wiley & Sons, Inc., New York (1999).
14. Putnam, Scott. Dissertation Work at The University of Tennessee-Knoxville (2005).
15. Selph, Curtis. Air Force Equilibrium Specific Impulse Code. United States Air Force (1992).
16. Hill, Phillip and Peterson, Carl, *Mechanics and Thermodynamics of Propulsion*, 2nd ed., Addison-Wesley Publishing Co., Massachusetts (1992).

APPENDICES

APPENDIX A: Flow Rate Calculation

Equations used in oxidizer mass flow rate chart calculation:

The mass flow rate is calculated as:

$$\dot{m}_{ox} = \frac{e * C * A_t * \sqrt{(2 * \rho * \Delta P)}}{\sqrt{(1-\beta^4)}} \qquad (17)$$

Beta ratio is the ratio of orifice plate hole diameter to pipe diameter:

$$\beta = \frac{d}{D} \qquad (18)$$

The density is calculated using the ideal gas law (temperature is assumed constant):

$$\rho = \frac{P_{up}}{\frac{R_u}{\mu_{ox}} * T_{ox}} \qquad (19)$$

The gas expansibility is determined as:

$$e = 1-(0.41+0.35*\beta^4)*\frac{\Delta P}{K * P_{up}} \qquad (20)$$

The discharge coefficient for flange taps is calculated as:

$$C = \left[0.598+0.468*\left(\beta^4+10*\beta^{12}\right)\right]*\sqrt{\left(1-\beta^4\right)}+(0.87+0.81*\beta^4)*\sqrt{\frac{\left(1-\beta^4\right)}{\mathrm{Re}_D}} \qquad (21)$$

The last term in the discharge coefficient calculation is small compared to the other term and is neglected in the code.

<u>MATLAB CODE</u>

```
%Matlab code used to create oxygen flow rate chart
%Clear memory
clear all;
clc;

%Orifice plate hole diameter (m)
d=0.00568706;
%Pipe diameter (m)
D=0.0157988;
%Beta ratio
b=d/D;
%Orifice and pipe diameters (m^2)
At=pi/4*d^2;
Ap=pi/4*D^2;
%Coefficients
k=1.29;
C=(0.598 +0.468*(b^4+10*b^12))*sqrt(1-b^4);
%Average upstream pressure (psig)
```

```
P=210;
%Convert to Pa
p1=(P+14.7)*6894.75729317;
%Temperature (K)---assumed value
T=297;
%Gas constant for oxygen (J/kg-K)
r=260;
%Standard pressure (Pa) and temperature (K)
pst=101325;
Tst=289;
%Density (kg/m^3)
rho=p1/r/T;

i=1;
dp(i)=0;
for i=1:1:101
%Expansion coefficient
e(i)=1-(0.41+0.35*b^4)*dp(i)/k/p1;
%Flow rate (kg/sec)
qm(i)=e(i)*C*At*sqrt(2*rho*dp(i))/sqrt(1-b^4);
%Other flow rates
qa(i)=qm(i)/rho;
qs(i)=qa(i)*p1*Tst/pst/T;
%Pressure differential (Pa)
dp(i+1)=dp(i)+6894.75729317;
end
%Print chart
fprintf('\n\t\t\t\t\t\tDifferential Pressure vs. Flow Rate\n')
fprintf('\t  0\t  1\t  2\t  3\t  4\t  5\t  6\t  7\t  8\t  9\t\n')
for i=1:10:100
fprintf('%2.0f\t%5.4f\t%5.4f\t%5.4f\t%5.4f\t%5.4f\t%5.4f\t%5.4f\t%5.4f\t%5.4f\t%5.4f\n
',i-1,qm(i),...
   qm(i+1),qm(i+2),qm(i+3),qm(i+4),qm(i+5),qm(i+6),qm(i+7),qm(i+8),qm(i+9))
end
fprintf('100\t%5.4f\n',qm(101))
```

SAMPLE CHART USING ABOVE CODE

Differential Pressure vs. Flow Rate (kg/sec) For P_{up}=210 psig

	0	1	2	3	4	5	6	7	8	9
0	0.0000	0.0078	0.0110	0.0135	0.0156	0.0174	0.0190	0.0205	0.0219	0.0232
10	0.0244	0.0255	0.0266	0.0277	0.0287	0.0296	0.0305	0.0314	0.0323	0.0331
20	0.0339	0.0347	0.0355	0.0362	0.0369	0.0376	0.0383	0.0390	0.0396	0.0403
30	0.0409	0.0415	0.0421	0.0427	0.0433	0.0438	0.0444	0.0449	0.0454	0.0459
40	0.0465	0.0470	0.0474	0.0479	0.0484	0.0489	0.0493	0.0498	0.0502	0.0507
50	0.0511	0.0515	0.0519	0.0523	0.0527	0.0531	0.0535	0.0539	0.0543	0.0547
60	0.0550	0.0554	0.0558	0.0561	0.0565	0.0568	0.0571	0.0575	0.0578	0.0581
70	0.0584	0.0588	0.0591	0.0594	0.0597	0.0600	0.0603	0.0606	0.0608	0.0611
80	0.0614	0.0617	0.0619	0.0622	0.0625	0.0627	0.0630	0.0632	0.0635	0.0637
90	0.0640	0.0642	0.0645	0.0647	0.0649	0.0652	0.0654	0.0656	0.0658	0.0660
100	0.0662									

APPENDIX B: HP VEE Screenshot with explanations

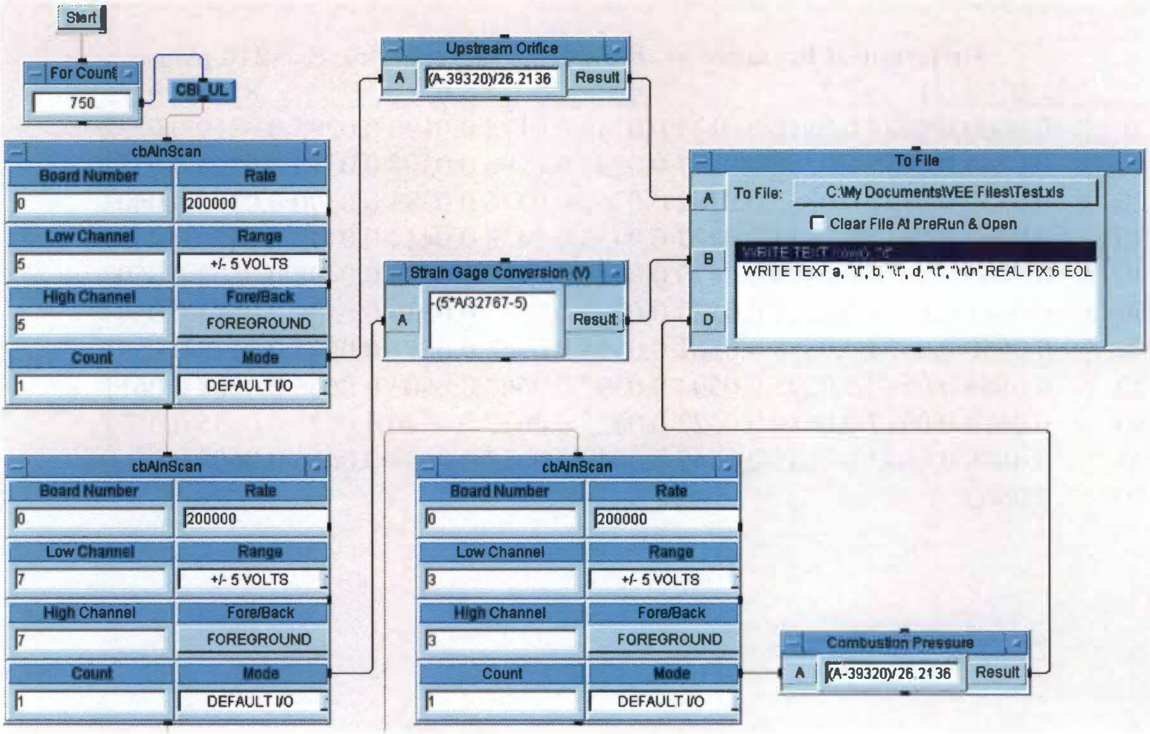

Figure 22: HP VEE Screenshot

The program is set to take a specific number of data points by the input value in the For Count box. At each time step, pressure values for each transducer and a thrust value are measured. The A/D card measures counts output, so this value must be converted to a desired value for use in data analysis. Each data point is taken and fed through a conversion calculation box that takes the data from counts to the desired range, being psig for the pressure transducers and mV for the strain gage. These values are saved in an Excel file in columns for ease of data analysis. Time data is stored as the leading column.

The total count range and the output range for the device determine the conversion calculation. For example, a pressure transducer conversion is determined as follows:

<u>Given</u>

Transducer Range (psig): 0 – 1000

Transducer voltage output range (V dc): 1 – 5

Counts for +/- 5 V: 0 – 65534

<u>Boundary Conditions</u>

Maximum pressure (1000 psig) occurs at 5 V (65534 counts)

Minimum pressure (0 psig) occurs at 1 V (39320 counts)

Conversion equation that satisfies boundary conditions:

$$P(psig) = \frac{Count - 39320}{26.136} \qquad (22)$$

APPENDIX C: Data reduction details

The regression rate as previously stated is the change in grain thickness per unit time:

$$\dot{r} = \frac{t_{g_f} - t_{g_i}}{t_b} \tag{23}$$

With the initial thickness and the burn time known, the only parameter needed to calculate the regression rate is the final grain thickness. It is assumed here that all burning takes place along the port, that is, there is no burning on the ends. The final grain thickness is determined using the density/mass/volume relation:

$$V = \frac{m}{\rho} \tag{24}$$

where the final mass and fuel density are known.

The volume can be thought of as the volume of a cylinder with a section deleted:

$$V = \pi * \frac{OD^2}{4} * L_g - \pi * \frac{D_f^{\,2}}{4} * L_g \tag{25}$$

Here the only unknown parameter is the final port diameter. This is calculated by inserting the volume relation into the aforementioned density/mass/volume relation. The final port diameter with some rearranging of the equation is given as:

$$D_f = \sqrt{\left(OD^2 - \frac{4 * M_f}{\pi \rho L_g} \right)} \tag{26}$$

The final grain thickness is calculated using the difference between the outer grain diameter and the final port diameter:

$$t_{g_f} = \frac{OD - \sqrt{\left(OD^2 - \frac{4 * M_f}{\pi \rho L_g} \right)}}{2} \tag{27}$$

With the final grain thickness calculated, the regression rate is easily determined.

Total impulse is found as the integrated result of thrust as a function of time. This is equivalent to the burned propellant mass multiplied by the equivalent exit velocity.

$$I = \int_{t=0}^{t=t_b} T * dt = M_p * u_{eq} \tag{28}$$

A Riemann squares approximation is used to determine the total impulse:

$$I = \sum_{i=0}^{i=t_b} \frac{1}{2} (T_{i+\Delta t} + T_i) * (t_{i+\Delta t} - t_i) \tag{29}$$

With knowledge of the burned propellant mass and the approximated total impulse the equivalent exit velocity is determined:

$$u_{eq} = \frac{I}{M_p} \tag{30}$$

Specific impulse for ideal expansion is lastly determined as the equivalent exit velocity over the acceleration due to gravity:

$$I_{sp} = \frac{I}{M_p * g_e} = \frac{u_{eq}}{g_e} \tag{31}$$

The mass flow rate of the fuel is easily calculated as the change in mass per unit time:

$$\dot{m}_f = \frac{M_{initial} - M_{final}}{t_b} \tag{32}$$

The mass flow rate of the propellant is the sum of the oxidizer and fuel flow rates:

$$\dot{m}_p = \dot{m}_{ox} + \dot{m}_f \tag{33}$$

With knowledge of the fuel mass flow rate the oxidizer to fuel ratio is calculated as:

$$O/F = \frac{\dot{m}_{ox}}{\dot{m}_f} \tag{34}$$

With this and the stoichiometric value, the equivalence ratio is determined:

$$\phi = \frac{O/F}{\left(O/F\right)_{stoich}} \tag{35}$$

The stoichiometric oxidizer to fuel ratio is determined using

$$\left(O/F\right)_{stoich} = \frac{moles_{ox}}{moles_f} * \frac{\mu_{ox}}{1mole_{ox}} * \frac{1mole_f}{\mu_f} \tag{36}$$

The molecular ratio is found from the stoichiometric chemical reaction balance:

$$1 * C_x H_y + aO_2 \rightarrow xCO_2 + \frac{y}{2} H_2O \tag{37}$$

Where a is the molecular ratio and is equivalent to:

$$a = x + \frac{y}{4} \tag{38}$$

The exit pressure to combustion (stagnation) pressure is:

$$\frac{P_e}{P_c} = \frac{14.7}{150} = 0.098 \tag{39}$$

The exit pressure in the thrust equation can be written in terms of the combustion pressure:

$$T = \dot{m}_{prop} * u_e + (0.098 * (P_c + 14.7) - P_a) A_e \tag{40}$$

The pressure thrust term can be easily calculated and removed with exit pressure given in terms of combustion pressure.

APPENDIX D: Summary of Test Results

Table 3: Test Summary

Test no.	Fuel	P_c (psig)	Thrust (N)	$\dot{m}_{ox}$ (kg/sec)	$\dot{r}$ (mm/sec)	I_{sp} (sec)	ϕ
1	Beeswax	32.3	23.5	x	1.33	x	x
2	Beeswax	38.1	25.0	x	1.32	x	x
3	Beeswax	50.7	48.7	x	1.61	x	x
4	Beeswax	39.3	29.7	x	1.30	x	x
14	Beeswax	141.0	108.4	x	2.81	x	x
20	Beeswax	178.0	135.0	x	2.76	x	x
22	Lard/Sponge	157.0	132.0	x	2.76	x	x
29	Beeswax	165.1	130.0	0.0397	2.85	141.6	0.23
30	Beeswax	149.3	115.8	0.0397	2.28	149.5	0.32
31	Beeswax	174.5	134.0	0.0395	3.26	130	0.19
32	Beeswax	155.5	113.0	0.0397	2.71	145	0.26
33	Beeswax	133.0	113.0	0.0380	1.94	160	0.41
34	Beeswax	154.5	113.0	0.0400	2.68	140.3	0.27
35	Beeswax	146.0	115.5	0.0256	2.41	173	0.20
36	Beeswax	178.0	113.0	0.0300	2.76	142	0.19
39	Beeswax	115.0	86.0	0.0240	2.40	132	0.19
40	Beeswax	104.0	79.0	0.0220	1.89	156.5	0.25
41	Beeswax	110.0	73.0	0.0220	2.35	118.7	0.18
47	Beeswax	109.0	80.6	0.0225	1.93	138	0.25
48	Beeswax	106.0	77.6	0.0218	1.92	151	0.24
49	Beeswax	233.0	129.0	0.0480	2.42	139.7	0.37
50	Beeswax	216.0	142.4	0.0525	2.14	167	0.45
52	Lard/Sponge	132.0	87.5	0.0254	1.41	164	0.42
53	Lard/Sponge	160.0	106.0	0.0265	1.83	166.5	0.30
56	Lard/Sponge	164.0	116.5	0.0348	1.68	195	0.46
58	Lard/Sponge	126.0	91.0	0.0366	2.30	164	0.31

VITA

Joshua David Scholes was born in Nashville, Tennessee on July 10, 1982. He attended Mt. Juliet High School in Mt. Juliet, TN where he graduated in 2000. He decided to pursue a degree in engineering at the University of Tennessee. The engineering decision stemmed from interests in mathematics and science. Concentrating in aerospace engineering, Joshua graduated with a Bachelors of Science in May 2004. He went on to pursue a Master of Science at the University of Tennessee where he graduated in December 2005. He is going on to work in the field of propulsion and engine testing.